ELSEVIER

Contents lists available at ScienceDirect

Journal of Wind Engineering & Industrial Aerodynamics

journal homepage: www.elsevier.com/locate/jweia



3D coupled wind-induced inelastic response of base-isolated tall buildings with eccentricity and biaxial interaction of hysteretic restoring base forces



Jingying Tian¹, Xinzhong Chen^{*}

National Wind Institute, Department of Civil, Environmental and Construction Engineering, Texas Tech University, Lubbock, TX, 79409-1023, USA

ARTICLE INFO

Keywords:
High-rise buildings
Inelastic response
Base-isolated tall building
Eccentricity
Biaxial hysteretic restoring force
Alongwind response
Crosswind response
Torsional response

ABSTRACT

This study presents an analysis framework for coupled inelastic response of base-isolated tall buildings with eccentricities of mass and resistance and coupled hysteretic restoring forces of base isolation system. The upper building motion is represented by lower modal displacements. The translational hysteretic restoring forces of base isolation system are described by a biaxial hysteretic model and the torsional restoring moment by a linear elastic model. The stochastic story wind forces of the upper building are represented in their cross power spectral matrix. Response history analysis is carried out to characterize the coupled responses of a square-shaped tall building with eccentricity in the center of resistance. The results showed that the eccentricity amplifies the alongwind response but has relatively less influence on the larger crosswind and torsional responses. The eccentricity has less influence on the inelastic response of based-isolated building as compared to the fixed-base building. The base isolation with inelastic response is more effective for building with eccentricity as compared to building without eccentricity. The biaxial interaction reduces the effect of eccentricity on base displacements but increases the effect on upper building response. The eccentricity and biaxal interaction result in fast growth of time-varying mean alongwind base displacement.

1. Introduction

Base isolation systems with nonlinear hysteretic restoring force characteristics have primarily been used for seismic design of low- and mid-rise buildings. For high-rise buildings, base isolation system can help to improve building performance in terms of comfort of occupants, functionality, non-damage to acceleration-sensitive contents and non-structural elements under seismic loading. In Japan, more than 200 base-isolated tall buildings with height greater than 60 m have been constructed. However, base isolation can reduce building modal frequencies thus leads to larger wind-induced response. There is of great importance to examine the performance of base-isolated tall buildings under strong wind excitations (see Table 11).

Several studies have addressed uncoupled wind-induced response of base-isolated tall buildings. Kareem (1997) studied alongwind elastic response of base-isolated buildings with passive dampers. Liang et al. (2002) investigated habitability characters of base-isolated tall buildings with hysteretic restoring force character under fluctuating wind excitation. Katagiri et al. (2011) examined the accuracy of reduced

building models in predicting uncoupled alongwind, crosswind, and torsional responses of base-isolated tall buildings through response history analysis. Katagiri et al. (2012) addressed the wind-induced responses of base-isolated tall buildings with consideration of motion-induced forces and point out the potential of unstable crosswind and torsional responses of lightly weighted buildings. Katagiri et al. (2014) investigated the response characteristics of isolation layer of base-isolated tall building through rain-flow method. Ogawa et al. (2016) discussed the characteristics of low-frequency shift of center displacement of isolation layer of base-isolated tall building under fluctuating wind force and proposed a prediction method of low-frequency shift from the resonant response component. Siringoringo and Fujino (2017) analyzed dynamic characteristics of a base-isolated building under typhoons using full-scale measurement data. The Japan Society of Seismic Isolated Buildings (JSSI) has developed guidelines for wind-resistant design of base-isolated buildings (JSSI, 2017). Feng and Chen (2019a and b) investigated the uncoupled alongwind and crosswind responses of base-isolated tall buildings with hysteretic restoring force characteristics quantified through response

^{*} Corresponding author.

E-mail addresses: 4221591@qq.com (J. Tian), xinzhong.chen@ttu.edu (X. Chen).

Currently, Lecturer, School of Civil Engineering, Changsha University of science and Technology, Changsha 410114, China.

time history analysis and statistical linearization approach. Feng and Chen (2021) presented a comprehensive study on the inelastic response of base-isolated tall buildings under nonstationary winds through response history analysis and statistical linearization approach.

Buildings having structural systems with noncoincident centers of

mass and resistance, or both, may undergo three-dimensional (3D) coupled motions when exposed to spatiotemporally varying wind loads (Kareem, 1985; Tallin and Ellingwood, 1985; Shimada et al., 1990; Islam et al., 1992; Flay et al., 1999; Chen and Kareem, 2005a; and b). The wind-induced elastic and inelastic responses of base isolated tall buildings with eccentricity has not yet been extensively investigated, while several earlier investigations have addressed the coupled lateral and torsional elastic and inelastic responses of base-isolated low- and middle-rise buildings under seismic excitations (Pan and Kelly, 1983; Nagarajaiah et al., 1991, 1993; Hwang and Hsu, 2000; Jangid and Kelly, 2000; Seguín et al., 2008; 2013; Bhatt, 2020; Shyamsunder et al., 2021). The effect of eccentricity on wind-induced building response is expected to be quite different from that on seismic response because of the difference in dynamic load excitations. The 3D dynamic wind loads are not affected by building eccentricity while the seismic loads are directly related to inertial loads that are influenced by building eccentricity. Another important factor influencing 3D coupled response of base-isolated buildings is the interaction of hysteretic restoring forces of base isolation system in three principal directions. A biaxial hysteretic restoring force model is often used to consider the biaxial interaction of translational hysteretic forces in two orthogonal directions with the corresponding translational displacements (Park et al., 1986; Wang and Wen, 2000; Harvey and Gavin, 2014), while the torsional restoring force

This study investigates 3D coupled inelastic responses of baseisolated tall buildings with eccentricities of mass and resistance and coupled hysteretic restoring forces of base isolation system. The upper building is modeled as a linear elastic multiple-degree-of-freedom (MDOF) shear building and is further represented by a reduced-order model through modal displacements. The coupled translational hysteretic restoring forces of base isolation system are modeled in a generalized biaxial Bouc-Wen model, while the torsional restoring force is represented by a linear elastic model. The story wind forces of the upper building are represented in their cross power spectral matrix. Response history analysis is carried out to characterize the coupled responses. A comprehensive parametric study is performed to explore the effects of base isolation, eccentricity of resistance center and biaxial interaction of hysteretic base restoring forces on time-varying mean and statistics of fluctuating building responses and their correlations. The results of this study help in developing improved understanding of coupled responses of base-isolated tall buildings with eccentricity and biaxial hysteretic restoring force character under strong wind loads.

is often represented by a linear elastic model.

2. Theoretical framework

2.1. Equations of motion

A multi-story base-isolated building with eccentricities of mass and resistance is considered. The coordinates of center of mass (C.M.) and center of resistance (C.R.) at *i*-th floor (i=1,2,...,N) are denoted as (e_{mxi},e_{myi}) , and (e_{xi},e_{yi}) as shown in Fig. 1, where the origin O at each floor is on the vertical z axis of cartesian coordinate system. The i-th floor has mass m_i , and moment of inertia around C.M., $I_{ic} = m_i r_i^2$, where r_i is the radius of gyration. The story stiffnesses in three directions are denoted as k_{xi} , k_{yi} and k_{00i} at C.R. The wind story forces and story torque acting at origin O are $P_{xi}(t)$, $P_{vi}(t)$ and $P_{0i}(t)$ in alongwind, crosswind and

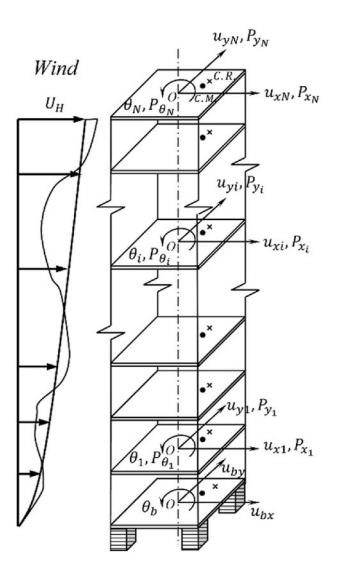


Fig. 1. Base-isolated building with eccentricities.

torsional directions, respectively. The *i*-th story translational and rotational displacements at origin O are denoted as $u_{xi}(t), u_{yi}(t)$ and $\theta_i(t)$, respectively.

The C.M. and C.R. of the base slab are located at (e_{mbx}, e_{mby}) and (e_{bx}, e_{by}) , respectively. The mass and moment of inertia around C.M. are denoted as m_b and $I_{ob} = m_b r_b^2$, where r_b is the radius of gyration. The restoring forces and torque at the C.R. of base slab are given as

$$F_{shx}^{'} = \eta_{hx} k_{hx} u_{hx}^{'} + (1 - \eta_{hx}) k_{hx} z_{x}^{'}$$
(1a)

$$F'_{sbv} = \eta_{bv} k_{by} u'_{bv} + (1 - \eta_{bv}) k_{by} z'_{v}$$
(1b)

$$M_{sb\theta}^{'} = k_{0b\theta}\theta_b$$
 (1c)

where u_{bx}', u_{by}' and θ_b are displacements at C.R.; z_x' and z_y' are hysteretic displacements; k_{bx}, k_{by} and $k_{0b\theta}$ are the stiffness at the C.R, of the base slab; η_{bx} and η_{bx} are the second stiffness ratios. It should be mentioned that the torsional stiffness of the isolation layer is generally related to the stiffness in both translational directions. As a result, the torsional stiffness also has nonlinear hysteretic properties. It is assumed that the restoring torque and torsional displacement are within the linear elastic range thus can be modeled in a linear elastic model.

When the translational hysteretic restoring forces are uncoupled, z_x' and z_y' are defined as the uniaxial Bouc-Wen model (Wen, 1976)

$$\dot{z}_{x}' = \dot{u}_{bx}' - z_{x}' |\dot{u}_{bx}'| |z_{x}'|^{n-1} \left[\beta_{x} + \gamma_{x} sgn(\dot{u}_{bx}'z_{x}') \right]$$
 (2a)

$$z'_{y} = u'_{by} - z'_{y} |u'_{by}| |z'_{y}|^{n-1} [\beta_{y} + \gamma_{y} sgn(u'_{by}z'_{y})]$$
 (2b)

where $\beta_x, \gamma_x, \beta_y, \gamma_y$ and n control the shape of hysteretic cycle; in this study, $\beta_x = \gamma_x, \beta_y = \gamma_y$ are used; The yielding displacements are $\Delta_x = (\beta_x + \gamma_x)^{-1/n}, \Delta_y = (\beta_y + \gamma_y)^{-1/n}$.

When the translational restoring forces are coupled, the following isotropic biaxial hysteretic model is used (Harvey and Gavin, 2014)

$$\dot{z}_{x}^{'} = \dot{u}_{bx}^{'} - z_{x}^{'}J; \dot{z}_{y}^{'} = \dot{u}_{by}^{'} - z_{y}^{'}J$$
 (3a)

$$J = \left\{ \left| \frac{\dot{u}_{bx}'}{\Delta_x} \right| \left| \frac{z_x'}{\Delta_x} \right| \left[\beta_0 + \gamma_0 sgn(\dot{u}_{bx}'z_x') \right] + \left| \frac{\dot{u}_{by}'}{\Delta_y} \right| \left| \frac{z_y'}{\Delta_y} \right| \left[\beta_0 + \gamma_0 sgn(\dot{u}_{by}'z_y') \right] \right\} \left[\left(\frac{z_x'}{\Delta_x} \right)^2 + \left(\frac{z_y'}{\Delta_y} \right)^2 \right]^{\frac{n-2}{2}}$$
(3b)

where $\beta_0 = \beta_x \Delta_x^n = \beta_y \Delta_y^n, \gamma_0 = \gamma_x \Delta_x^n = \gamma_y \Delta_y^n$.

The normalized accumulated dissipated hysteretic energy until time instant t can be defined as (Lee and Hong, 2010)

$$E_{nx} = \frac{(1 - \eta_{bx})}{\Delta_x^2} \int_0^t z_x' \dot{u}_{bx}' dt; E_{ny} = \frac{(1 - \eta_{by})}{\Delta_y^2} \int_0^t z_y' \dot{u}_{by}' dt$$
 (4)

In the matrix format, the hysteretic restoring forces at C.R. of base slab are represented as

$$F_{sb}^{'} = \eta_b K_b u_b^{'} + (I - \eta_b) K_b z^{'}$$
 (5a)

$$C_b = \operatorname{diag}(c_{bx}, c_{by}, c_{b\theta}); \mathbf{R} = \begin{bmatrix} \mathbf{r} & \mathbf{0} & \mathbf{0} \\ \mathbf{0} & \mathbf{r} & \mathbf{0} \\ \mathbf{0} & \mathbf{0} & \mathbf{r} \end{bmatrix}; \mathbf{r} = \begin{bmatrix} 1 \\ \vdots \\ 1 \end{bmatrix};$$

$$P_s(t) = \{ P_{s1}(t), ..., P_{sN}(t) \}^T (s = x, y, \theta);$$

$$P_{\theta}(t) / r = \{P_{\theta 1}(t)/r_1, ..., P_{\theta N}(t)/r_N\}^T$$

where $u = \{u_x^T, u_y^T, u_\theta^T\}^T$ are the building displacements vector relative to the base; M, C and K are the mass, damping and stiffness matrices of the upper building; m_i is the mass of i-th story; $m_{\theta\theta i} = m_i (1 + e_{mxi}^2/r_i^2 + e_{myi}^2/r_i^2)$; M_b and C_b are the mass and linear damping matrices of base;

$$\mathbf{K}_{b} = \operatorname{diag}(k_{bx}, k_{by}, k_{0b\theta} / r_{b}^{2}); \boldsymbol{\eta}_{b} = \operatorname{diag}(\eta_{bx}, \eta_{by}, 1); \quad \mathbf{F}'_{sb} = \left\{ F'_{sbx}, F'_{sby}, M'_{sb\theta} / r_{b} \right\}^{T}; \quad \mathbf{z}' = \left\{ z'_{x}, z'_{y}, z'_{\theta} \right\}^{T} = \left\{ z'_{x}, z'_{y}, u'_{b\theta} \right\}^{T};$$

$$\mathbf{I} = \operatorname{diag}(1, \dots, 1); \boldsymbol{u}'_{b} = \left\{ u'_{bx}, u'_{by}, u'_{b\theta} \right\}^{T} = \left\{ u'_{bx}, u'_{by}, r_{b}\theta_{b} \right\}^{T} \tag{5b}$$

The restoring forces vector and displacements vector at the origin of base slab are related to those at the C.R. as

$$F_{sb} = e_b^T F_{sb}'; u_b' = e_b u_b. \tag{6a}$$

$$\mathbf{F}_{sb} = \left\{ F_{sbx}, F_{sby}, F_{sb\theta} \right\}^{T}; \mathbf{u}_{b} = \left\{ u_{bx}, u_{by}, u_{b\theta} \right\}^{T}; \mathbf{e}_{b} = \begin{bmatrix} 1 & 0 & -e_{by}/r_{b} \\ 0 & 1 & e_{bx}/r_{b} \\ 0 & 0 & 1 \end{bmatrix}$$
 (6b)

Thus, the hysteretic restoring forces and base displacements at the origin of base slab are related as

$$F_{sb} = e_b^T \eta_b K_b e_b u_b + e_b^T (I - \eta_b) K_b z'$$

$$(7)$$

It is obvious that the eccentricity of base slab leads to a hysteretic relation of torsional moment around the origin with translational and torsional displacements at the origin of base slab.

The equations of motion of the base-isolated building are

$$MR\ddot{u}_b + M\ddot{u} + C\dot{u} + Ku = P(t)$$
(8a)

$$(\mathbf{M}_h + \mathbf{R}^T \mathbf{M} \mathbf{R}) \ddot{\mathbf{u}}_h + \mathbf{R}^T \mathbf{M} \ddot{\mathbf{u}} + \mathbf{C}_h \dot{\mathbf{u}}_h + \mathbf{F}_{sh} = \mathbf{R}^T \mathbf{P}(t)$$
(8b)

$$M = \begin{bmatrix} M_{xx} & 0 & M_{x\theta} \\ 0 & M_{yy} & M_{y\theta} \\ M_{x\theta} & M_{y\theta} & M_{\theta\theta} \end{bmatrix}; K = \begin{bmatrix} K_{xx} & 0 & K_{x\theta} \\ 0 & K_{yy} & K_{y\theta} \\ K_{\theta x} & K_{\theta y} & K_{\theta\theta} \end{bmatrix}; P(t) = \begin{bmatrix} P_x(t) \\ P_y(t) \\ P_{\theta}(t)/r \end{bmatrix};$$

 $\mathbf{M}_{ss} = \operatorname{diag}(m_1, ..., m_N) \ (s = x, y); \mathbf{M}_{\theta\theta} = \operatorname{diag}(m_{\theta\theta 1}, ..., m_{\theta\theta N});$

$$\mathbf{M_b} = \begin{bmatrix} m_b & 0 & -(e_{mby}/r_b)m_b \\ 0 & m_b & (e_{mbx}/r_b)m_b \\ -(e_{mby}/r_b)m_b & (e_{mbx}/r_b)m_b & m_{b\theta} \end{bmatrix}$$
(8c)

 $m_{b\theta}=m_b(1+e_{mbx}^2/r_b^2+e_{mby}^2/r_b^2);$ c_{bx},c_{by} and $c_{b\theta}$ are the damping coefficients of base; P(t) is the story wind forces vector; R reflects the displacements of upper building resulted from unit displacement in base. The expressions of mass and stiffness matrices $M_{x\theta}=M_{\theta x}'$, $M_{y\theta}=M_{\theta y}'$, K_{ss} $(s=x,y,\theta)$, $K_{x\theta}=K_{\theta x}'$ and $K_{y\theta}=K_{\theta y}'$ are omitted here for the sake of brevity. The damping matrix of upper building is assumed to be proportional to stiffness matrix and is determined according to the first modal damping ratio of upper building. As being pointed by Ryan and Polanco (2008), the damping matrix as proportional to mass matrix can result in undesirable large damping ratio of the first mode of base-isolated building.

It is evident that by setting the base displacement $u_b(t)=\mathbf{0}$, the equations of building motion become those for fixed-base building. The mode frequencies and shapes of fixed-base building are determined through the solution of following eigenvalue problem:

$$K\varphi_i = \omega_i^2 M\varphi_i \tag{9}$$

where ω_j (j=1,2,...,3N) is the *j*-th modal frequency; $\varphi_j = \{\varphi_{jx}^T, \varphi_{jy}^T, \varphi_{j\theta}^T\}^T$ is the *j*-th mode shape. The equations of motion of building without eccentricity are uncoupled for the displacements in three principal directions, where the mode shapes are one dimensional.

The upper building displacements of base-isolated building relative to base is represented in first 3S $(S \le N)$ modal displacements as

$$\boldsymbol{u}(t) \approx \sum_{i=1}^{3S} \boldsymbol{\varphi}_{i} q_{i}(t) = \boldsymbol{\varphi} \boldsymbol{q}(t)$$
 (10)

where φ is the 3S mode shapes of fixed-base building; q(t) is the generalized displacements.

Accordingly, the equations of motion are reduced to

$$\overline{M}\ddot{\overline{q}}(t) + \overline{C}\dot{\overline{q}}(t) + \overline{K}_{1}\overline{q}(t) + \overline{K}_{2}z'(t) = Q(t)$$
(11a)

$$\overline{M} = \begin{bmatrix} M_b + R^T M R & R^T M \varphi \\ \varphi^T M R & M^* \end{bmatrix}; \overline{C} = \begin{bmatrix} C_b & 0 \\ 0 & C^* \end{bmatrix}; \overline{K}_1 = \begin{bmatrix} e_b^T \eta_b K_b e_b & 0 \\ 0 & K^* \end{bmatrix}; \overline{K}_2 = \begin{bmatrix} e_b^T (1 - \eta_b) K_b \\ 0 \end{bmatrix}; ; \overline{q}(t) = \begin{Bmatrix} u_b(t) \\ q(t) \end{Bmatrix}; \underline{Q}(t) = \begin{Bmatrix} R^T \\ \varphi^T \end{Bmatrix} P(t) = \begin{Bmatrix} Q_F(t) \\ Q_0(t) \end{Bmatrix}$$
(11b)

where $M^* = \varphi^T M \varphi$, $C^* = \varphi^T C \varphi$, $K^* = \varphi^T K \varphi$ are the generalized mass, damping and stiffness matrices of the corresponding fixed-base building, respectively; $Q_F(t) = R^T P(t)$ and $Q_0(t) = \varphi^T P(t)$ are the base shear forces and torque, and the generalized forces of the upper building.

The equations of motion can be represented in state-space equations as

$$\dot{\mathbf{v}}(t) = \mathbf{g}(\mathbf{v}(t)) + \overline{\mathbf{D}}\mathbf{Q}(t) \tag{12a}$$

$$g(v(t)) = \begin{bmatrix} -\overline{M}^{-1}\overline{C}\dot{q} - \overline{M}^{-1}\overline{K}_{1}\overline{q} - \overline{M}^{-1}\overline{K}_{2}z' \\ \left\{ \dot{u}'_{bx} - z'_{x}J, \dot{u}'_{by} - z'_{y}J, \dot{u}'_{b\theta} \right\}^{T} \end{bmatrix}; v(t) = \begin{bmatrix} \overline{q} \\ \overline{q}z' \end{bmatrix}; \overline{D} = \begin{bmatrix} \mathbf{0} \\ \overline{M}^{-1} \\ \mathbf{0} \end{bmatrix}$$

Once the generalized displacements are quantified, any other building response of interest, R(t), is given by

$$R(t) \approx \sum_{j=1}^{3S} R_j(t) = \sum_{j=1}^{3S} \Gamma_j q_j(t)$$
 (13a)

$$\Gamma_{j} = \left(2\pi f_{j}\right)^{2} \sum_{i=1}^{N} \left(\mu_{xi} m_{i} \varphi_{ixc,j} + \mu_{yi} m_{i} \varphi_{iyc,j} + \mu_{\theta i} m_{i} \varphi_{i\theta c,j}\right) \tag{14a}$$

where $R_j(t) = \Gamma_j q_j(t)$ is the contribution of the j-th mode to R(t); Γ_j is the participation coefficient of the j-th mode; $\varphi_{ixc,j}, \varphi_{iyc,j}$ and $\varphi_{i\theta c,j}$ are the j-th modal shapes in terms of i-th story displacements at C.M.; μ_{si} ($s=x,y,\theta$) are the influence line coefficients, representing the static response of R caused by the unit loading at i-th floor C.M. in s direction; and f_j is j-th modal frequency of the fixed-base building.

The yielding of base-isolation system causes base displacement drift attributed to the existence of mean (static) wind load until reaching the steady-state displacement, which is determined by the static load and post-yielding stiffness of the system (Baber, 1984; Feng and Chen, 2019a). The state-state displacement is determined by setting the hysteretic displacements $z^{'}(t) = 0$. Accordingly, Eq. (8) leads to

$$Ku = \overline{P} \tag{13b}$$

$$e_b^T \eta_b K_b e_b u_b = R^T \overline{P} \tag{13c}$$

and in modal coordinates, it gives

$$\overline{K}_1 \mu_{\overline{q}} = \mu_{Q} \tag{14b}$$

where \overline{P} is the mean (static) story forces; and μ_Q is the mean value of O(t).

2.2. Wind loading model

The story wind force coefficients of i-th floor, coefficients of base bending moments and base torque are defined as

$$C_{P_{si}}(t) = \frac{P_{si}(t)}{0.5\rho U_H^2 B H_0}; \ C_{P_{\theta i}}(t) = \frac{P_{\theta i}(t)}{0.5\rho U_H^2 B^2 H_0} \tag{15a}$$

$$C_{M_s}(t) = \frac{M_s(t)}{0.5\rho U_H^2 B H^2}; C_{M_\theta}(t) = \frac{M_\theta(t)}{0.5\rho U_H^2 B^2 H}$$
 (15b)

Where $P_{si}(t)$ ($s=x,y,\theta$) are the i-th story forces; $F_s(t)$ and $M_s(t)$ (s=x,y) are the base shear forces and bending moments; $M_{\theta}(t)$ is the base torque; $\rho=1.225 {\rm kg/m^3}$ is air density; B is the building width; H_0 is the story height; H is the building height; H is the 10-min mean wind speed at building top.

In this study, the mean (static) alongwind story force coefficient is defined as

$$\overline{C}_{P_{xi}} = \overline{C}_D \left(\frac{z_i}{H}\right)^{2\alpha_i} \tag{16}$$

where \overline{C}_D is mean drag force coefficient and assumed to be constant over the building height, which is related to the base bending moment coefficient \overline{C}_{M_x} as $\overline{C}_D = 2\overline{C}_{M_x}(\alpha_s+1)$; α_s is wind load profile coefficient and is 1/4 in this study; $\overline{C}_{M_x} = 0.5937$ and $\alpha_s = 1/4$ are determined from the wind tunnel data for a square-shaped tall building model (TPU Aerodynamic Database, 2021); z_i is the elevation of *i*-th floor above the ground.

According to wind tunnel data of dynamic pressures on a squareshaped tall building model (TPU Aerodynamic Database, 2021), it is assumed that the power spectral density functions (PSDs) of story force coefficients at different heights, but same direction have the same shape

$$S_{C_{P_{s_i}}}(f) = \sigma_{C_{P_{s_0}}}^2 S_{C_{P_{s_0}}}(f)(s = x, y, \theta)$$
(17)

where $\sigma_{C_{P_{sl}}}$ is the standard deviation (STD) of $C_{P_{sl}}(t)$; and $S_{C_{P_{s0}}}(f)$ is calculated from the PSD of base bending moment or torque $S_{C_{M_s}}(f)$ ($s=x,y,\theta$) as

$$S_{C_{P_{s0}}}(f) = \left(\frac{H}{H_0}\right)^2 S_{C_{M_s}}(f) / \sum_{i=1}^{N} \sum_{j=1}^{N} \sigma_{C_{P_{si}}} \sigma_{C_{P_{sj}}} Coh_{sij}(f) \left(\frac{z_i}{H}\right) \left(\frac{z_j}{H}\right) (s = x, y)$$
(18a)

$$S_{C_{P_{\theta 0}}}(f) = \left(\frac{H}{H_0}\right)^2 S_{C_{M_{\theta}}}(f) / \sum_{i=1}^{N} \sum_{j=1}^{N} \sigma_{C_{P_{\theta i}}} \sigma_{C_{P_{\theta j}}} Coh_{\theta ij}(f)$$
(18b)

where $Coh_{sij}(f)$ ($s = x, y, \theta$) are the coherence functions between *i*-th and

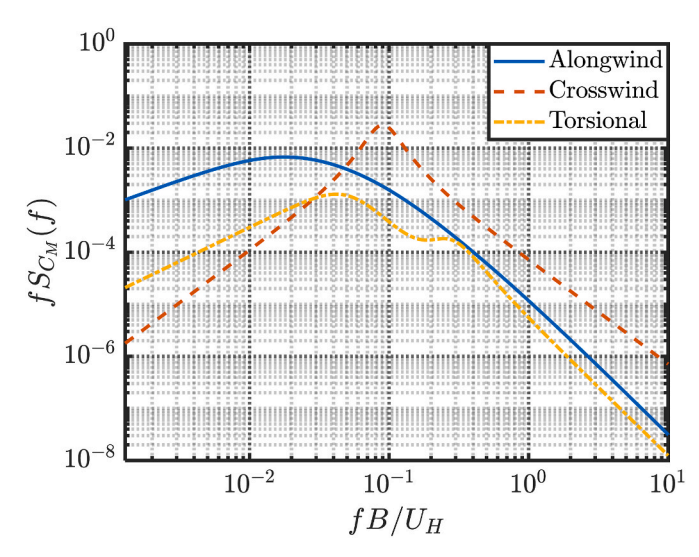


Fig. 2. PSDs of base bending moment and base torque coefficients.

j-th story forces in s direction.

In this study, the PSDs of alongwind and crosswind base bending moment coefficients are determined from AIJ recommendation (AIJ, 2004) but with $\sigma_{C_{M_x}} = 0.1363$ and $\sigma_{C_{M_y}} = 0.1746$. A power spectral model of torsional base torque coefficient (Kijewski and Kareem, 1998) is fitted from wind tunnel data with $\sigma_{C_{M_0}} = 0.0485$. The STDs of story forces and coherence functions and PSDs of base bending moments and torque coefficients are given in Appendix, which are established according to wind tunnel data of dynamic pressures on a square-shaped tall building model (TPU Aerodynamic Database, 2021).

The cross PSD (CPSD) of i-th story crosswind and j-th story torsional force coefficients is modeled as

$$S_{C_{P_{yi}}C_{P_{gj}}}(f) = Coh_{y00}(f)\sqrt{Coh_{yij}(f)Coh_{\theta ij}(f)}\sqrt{S_{C_{P_{yi}}}(f)S_{C_{P_{gj}}}(f)}$$
(19)

Accordingly, the CPSD of crosswind base bending moment coefficient and base torque coefficient is expressed as

$$S_{C_{M_y}C_{M_{\theta}}}(f) = \frac{H_0^2}{H^2} \sum_{i=1}^{N} \sum_{i=1}^{N} S_{C_{P_{yi}}C_{P_{\theta j}}}(f) \left(\frac{z_i}{H}\right)$$
 (20)

which can be used to determine the complex-valued coherence $Coh_{y\neq 0}(f)$. According to the wind tunnel data of a square-shaped tall building, the magnitude and phase of the coherence model are determined as shown in Appendix. The PSDs of base bending moment coefficients and base torque coefficient are shown in Fig. 2. It is noted that the vortex lock-in reduced wind speed is around $U_H/fB = 11.11$. The wind speed addressed in this study is much lower than this critical wind speed of vortex-induced vibration. Therefore, the aerodynamic damping effect and vortex-induced vibration are not considered in this study.

The PSD matrix of the force vector Q(t) is then computed as

$$S_{\boldsymbol{Q}}(f) = [\boldsymbol{R}, \boldsymbol{\varphi}]^T S_{\boldsymbol{P}\boldsymbol{P}}(f)[\boldsymbol{R}, \boldsymbol{\varphi}]$$
(21)

where $S_{PP}(f)$ is the PSD matrix of wind loading vector P(t).

3. Building model

A 50-story tall building with a square cross section is considered. The building height H=200 m, width B=40 m and building density is 192 kg/m³. The building has no eccentricity in C.M., but eccentricity in C.R. The story mass $m_i=1.2288\times 10^6$ kg and moment of inertia about origin $I_{iC}=m_ir_i^2$; $r_i=r=B/2/\sqrt{6}=8.1650$ m. The eccentricity of C.R. at each floor level is same, i.e., $e_{xi}/r_i=e_{yi}/r_i=-0.40$.

The fixed-base upper building without eccentricity has fundamental frequencies $f_{0x1}=0.210$ Hz, $f_{0y1}=0.252$ Hz, and $f_{0\theta1}=0.300$ Hz. The corresponding mode shapes follow linear functions along the building height, i.e., $\varphi_{0x1}(z_i)=\varphi_{0y1}(z_i)=\varphi_{0\theta1}(z_i)=z_i/H$. It is noted that torsional displacement is referred to as $u_{\theta i}=r_i\theta_i$. The story stiffnesses of the shear building are determined from fundamental frequencies and mode shapes as

$$k_{si} = \frac{(2\pi f_{0s1})^2}{\varphi_{0s1}(z_i) - \varphi_{0s1}(z_{i-1})} \sum_{j=i}^{N} m_j \varphi_{0s1}(z_j), (s = x, y)$$
(22a)

$$k_{0\theta i} = \frac{(2\pi f_{0\theta i})^2}{\varphi_{0\theta 1}(z_i) - \varphi_{0\theta 1}(z_{i-1})} \sum_{j=i}^{N} m_j \varphi_{0\theta 1}(z_j)$$
(22b)

Table 1Dynamic properties of base isolation system.

Direction	m_b (kg) or I_{0b} (kg·m ²)	$k_{bs} (kN/m)$ or $k_{0b\theta} (kN \cdot m)$	f_{bs} (Hz)	C_{bs}	η_{bs}
x	4.08(10 ⁵)	5.53 (10 ⁵)	0.480	0	0.12
у	4.08 (10 ⁵)	8.25 (10 ⁵)	0.580	0	0.12
θ	$2.72 (10^7)$	$7.23\ (10^{10})$	0.670	0	1

The first modal damping ratios of the fixed-base building without eccentricity are $\xi_{0x1}=\xi_{0y1}=\xi_{0\theta1}=1\%$.

The yielding displacements of base isolation system in two translational directions are $\Delta_x=\Delta_y=0.025$ m. The restoring forcesdisplacements are described by the biaxial hysteretic Bouc-Wen model with $\beta_s=\gamma_s=0.5\Delta_s^n$ (s=x,y) and n=6. The linear damping of base in three directions is neglected. Feng and Chen (2019a) have investigated the influence of damping ratio of base isolation system on uncoupled building responses. It has little influence on the upper building displacement when the base isolation system shows obvious inelastic response at higher wind speeds with the development of additional hysteretic damping. The dynamic properties of base isolation system are listed in Table 1. The eccentricity of C.R. of base isolation system is $e_{bx}/r_b=e_{by}/r_b=-0.40$, where $r_b=\sqrt{I_{ob}/m_b}=8.1650$ m. The eccentricity of C.R. of base isolation system is same as the upper building.

4. Reduced-order building model

4.1. Fixed-base building

The modal analysis is firstly carried out for the fixed-base building without eccentricity. Dynamic modal properties of first 3 modes in each direction are listed in Table 2, where the mode shapes are normalized with unit building top displacement. The damping matrix in each direction is assumed to be proportional to the corresponding stiffness matrix and determined using the first modal damping ratio of the direction, which can avoid the undesirable suppression of the first modal response when the building is base isolated (Ryan and Polanco, 2008). Accordingly, the i-th modal damping ratio in the s-direction (i = 1,2,3, and $s = x,y,\theta$) is given by $\xi_{0si} = (f_{0si}/f_{0s1})\xi_{0s1}$ (Chopra, 2017), which is proportional to modal frequency, where f_{0si} and ξ_{0si} are the i-th modal frequency and damping ratio. The mode shapes in three directions are the same and shown in Fig. 3.

Table 3 shows the dynamic modal properties of the fixed-base building with eccentricity in C.R., where the mode shapes are normalized with unit top displacement in dominant direction. The three fundamental mode shapes are shown in Fig. 4and Fig. 5 which are coupled with dominant motion in x, y and θ directions, respectively. The modal frequencies are reduced by 8% and 7% in x and y directions respectively and increased by 17% in θ direction, as compared to the fixed-base building without eccentricity.

The generalized mass is calculated as

$$M_{0i} = \sum_{i=1}^{N} \left(m_{ij} \varphi_{jxc,i}^{2} + m_{j} \varphi_{jyc,i}^{2} + m_{j} \varphi_{j\theta c,i}^{2} \right)$$
 (23a)

$$M_{0si} = \sum_{i=1}^{N} m_j \varphi_{jsc,i}^2, (s = x, y, \theta)$$
 (23b)

where M_{0i} and M_{0si} are the total generalized mass and the generalized mass component associated with mode shape in s direction ($s = x, y, \theta$) of i-th mode. The dominate vibration components can be readily identified from these generalized mass components.

4.2. Base-isolated building

The base-isolated building has 51 DOFs in each direction including 50 DOFs of upper building. In the case without eccentricity, the mode shapes in three directions are uncoupled. The damping matrix of base-isolated building is nonclassical in general. Since the damping of base isolation system is assumed to be low and is not included in this study, the real modal analysis can lead to almost the same results as those from complex modal analysis. The modal properties with initial stiffness of the base isolation system are listed in Table 4. As compared to fixed-base building without eccentricity, the three fundamental modal frequencies

Table 2Dynamic modal properties of fixed-base building without eccentricity.

Direction (s)	x			у			θ		
Mode	1	2	3	1	2	3	1	2	3
f_{0si} (Hz)	0.210	0.514	0.813	0.252	0.617	0.976	0.300	0.735	1.162
$M_{0i} (\times 10^7 \text{ kg})$	2.11	1.00	0.76	2.11	1.00	0.76	2.11	1.00	0.76
ξ _{0si} (%)	1.00	2.45	3.87	1.00	2.45	3.87	1.00	2.45	3.87

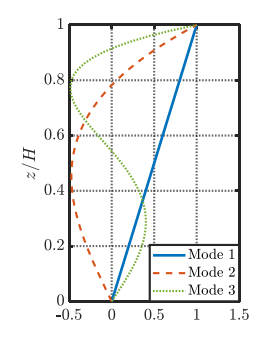


Fig. 3. Mode shapes of fixed-base building without eccentricity.

are reduced by 7%. The damping ratios are reduced by 20%. The mode shapes of the upper building are also affected by base isolation system.

The modal analysis by using reduced-order models of the upper building is also carried out. The upper building is respectively represented by only one mode, two and three modes in each direction, referred to as 2DOFs, 3DOFs and 4DOFs models (including the one DOF of the base) as compared to 51DOFs model. The results are also shown in Table 4. The first three mode shapes with different reduced-order models are show in Fig. 6 and are compared with those from 51DOFs model. The mode shapes are normalized by setting the building top displacement relative to base to be one. The mode shapes in all three directions are the same. It is evident that the reduced-order building model with (n+1) DOFs in each direction can give accurate representation of the first n modes of the base-isolated building in each direction in terms of modal frequencies, damping ratios, modal shapes, and

Table 3 Dynamic modal properties of fixed-base building with eccentricity.

Dominant direction (s)	x			у			θ		
Mode	1	2	3	1	2	3	1	2	3
f_{0si} (Hz)	0.193	0.473	0.748	0.235	0.576	0.911	0.350	0.856	1.354
$M_{0i} \ (\times \ 10^7 \ \mathrm{kg})$	2.73	1.29	0.98	2.85	1.35	1.03	2.61	1.24	0.94
$M_{0xi} \ (\times 10^7 \ \text{kg})$	2.11	1.00	0.76	0.53	0.25	0.19	0.11	0.05	0.04
$M_{0yi} \ (\times 10^7 \ \text{kg})$	0.30	0.14	0.11	2.11	1.00	0.76	0.40	0.19	0.14
$M_{0\theta i}$ (×10 ⁷ kg)	0.32	0.15	0.11	0.22	0.10	0.08	2.11	1.00	0.76
ξ_{0si} (%)	1.00	2.45	3.87	1.00	2.45	3.87	1.00	2.45	3.87

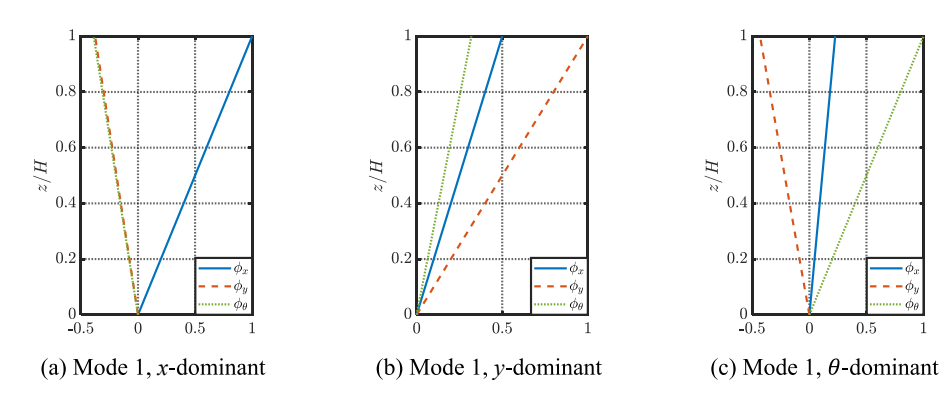


Fig. 4. Coupled mode shapes of fixed-base building with eccentricity.

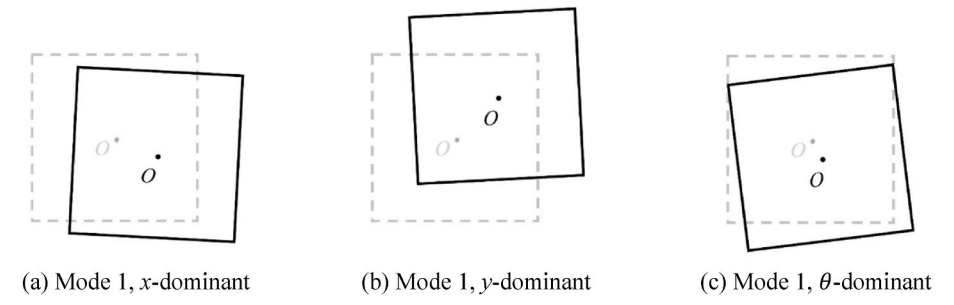


Fig. 5. Section view of coupled mode shapes of fixed-base building with eccentricity.

Table 4Dynamic modal properties of base-isolated building without eccentricity (initial stiffness).

Direction (s)		x			у	у		θ		
Mode		1	2	3	1	2	3	1	2	3
f _{si} (Hz)	51DOFs	0.196	0.484	0.769	0.235	0.582	0.924	0.279	0.691	1.096
	2DOFs	0.196	1.027	/	0.235	1.251	/	0.279	1.443	/
	3DOFs	0.196	0.485	1.459	0.235	0.583	1.775	0.279	0.692	2.054
	4DOFs	0196	0.485	0.772	0.235	0.583	0.928	0.279	0.691	1.101
M_{si}	51DOFs	2.89	0.84	1.21	2.86	0.85	1.20	2.93	0.84	1.23
(10^7 kg)	2DOFs	2.82	0.64	/	2.79	0.64	/	2.85	0.64	/
ν ο.	3DOFs	2.91	0.79	2.63	2.88	0.80	2.60	2.95	0.79	2.66
	4DOFs	2.89	0.86	1.02	2.86	0.86	1.01	2.92	0.86	1.03
ξ_{si} (%)	51DOFs	0.80	2.05	3.32	0.81	2.06	3.33	0.80	2.05	3.32
	2DOF	0.80	0.67	/	0.80	0.67	/	0.80	0.67	/
	3DOFs	0.80	2.07	1.68	0.80	2.07	1.68	0.80	2.07	1.68
	4DOFs	0.80	2.06	3.37	0.80	2.06	3.37	0.80	2.06	3.37
u_{bs}	51DOFs	0.105	-0.125	0.220	0.101	-0.121	0.212	0.890	-1.047	1.858
	2DOFs	0.103	-0.645	/	0.099	-0.646	/	0.876	-5.260	/
	3DOFs	0.105	-0.118	1.738	0.101	-0.115	-1.730	0.892	-0.989	-14.27
	4DOFs	0.105	-0.125	0.191	0.101	-0.121	0.185	0.889	-1.049	1.609

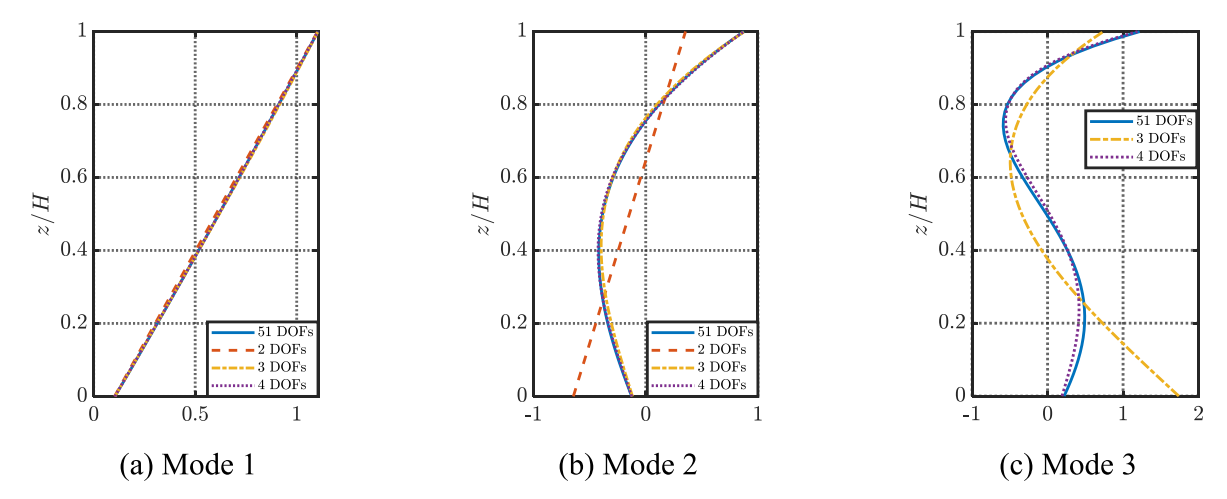


Fig. 6. Mode shapes of base-isolated building without eccentricity in x direction (initial stiffness).

Table 5Dynamic modal properties of base-isolated building with eccentricity (initial stiffness).

Dominant direc	ction	x			у			θ		
Mode		1	2	3	1	2	3	1	2	3
f _i (Hz)	51DOFs	0.180	0.445	0.706	0.219	0.543	0.862	0.325	0.806	1.279
	2DOFs	0.180	0.940	/	0.219	1.159	/	0.325	1.701	/
	3DOFs	0.180	0.446	1.336	0.219	0.544	1.646	0.325	0.807	2.418
	4DOFs	0.180	0.445	0.709	0.219	0.544	0.866	0.325	0.806	1.284
M_i	51DOFs	3.75	1.09	1.56	3.90	1.15	1.66	3.66	1.04	1.52
(10^7 kg)	2DOFs	3.66	0.83	/	3.80	0.89	/	3.55	0.82	/
, 0.	3DOFs	3.77	1.02	3.41	3.92	1.08	3.59	3.68	0.98	3.36
	4DOFs	3.74	1.11	1.31	3.89	1.17	1.39	3.65	1.06	1.29
ξ_i (%)	51DOFs	0.80	2.05	3.31	0.81	2.06	3.32	0.80	2.05	3.31
	2DOFs	0.80	0.68	/	0.81	0.67	/	0.80	0.68	/
	3DOFs	0.80	2.07	1.69	0.81	2.08	1.67	0.80	2.07	1.69
	4DOFs	0.80	2.06	3.36	0.81	2.06	3.37	0.80	2.06	3.36
u_{bx}	51DOFs	0.105	-0.125	0.220	0.052	-0.062	0.109	0.022	-0.029	0.054
	2DOFs	0.104	-0.645	/	0.051	-0.333	/	0.022	-0.148	/
	3DOFs	0.106	-0.118	1.737	0.052	-0.059	0.886	0.022	-0.024	0.399
	4DOFs	0.105	-0.125	0.191	0.052	-0.062	0.095	0.022	-0.029	0.037
u_{by}	51DOFs	-0.039	0.047	-0.082	0.102	-0.122	0.218	-0.042	0.047	-0.095
-	2DOFs	-0.039	0.240	/	0.100	-0.646	/	-0.041	0.304	/
	3DOFs	-0.039	0.044	-0.646	0.102	-0.116	1.729	-0.042	0.046	-0.815
	4DOFs	-0.039	0.047	-0.071	0.102	-0.122	0.189	-0.042	0.048	-0.073
$u_{b\theta}$	51DOFs	-0.042	0.050	-0.089	0.035	-0.041	0.070	0.109	-0.129	0.223
	2DOFs	-0.042	0.261	/	0.035	-0.229	/	0.107	-0.645	/
	3DOFs	-0.042	0.047	-0.698	0.035	-0.039	0.603	0.110	-0.122	1.743
	4DOFs	-0.042	0.050	-0.077	0.035	-0.042	0.061	0.109	-0.129	0.201

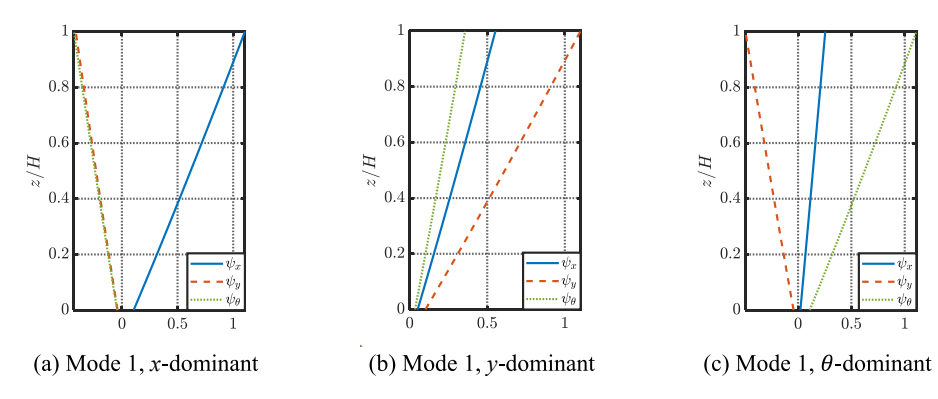


Fig. 7. Coupled mode shapes of base-isolated building with eccentricity.

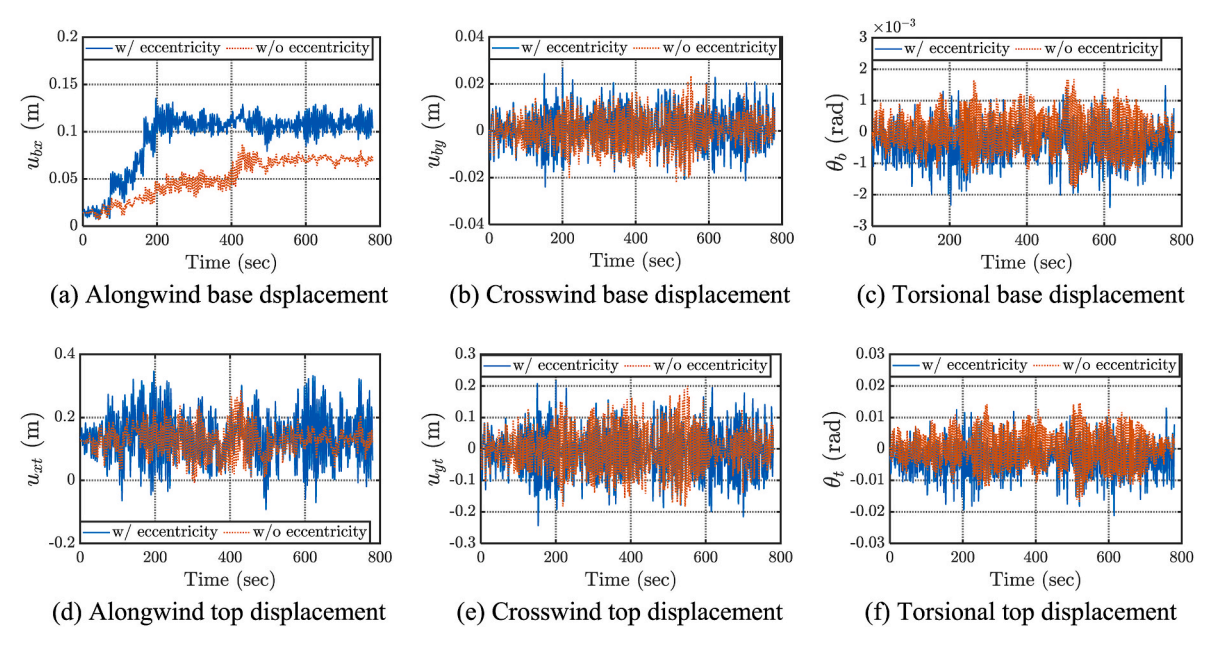


Fig. 8. Response time history samples ($U_H = 40 \text{ m/s}$).

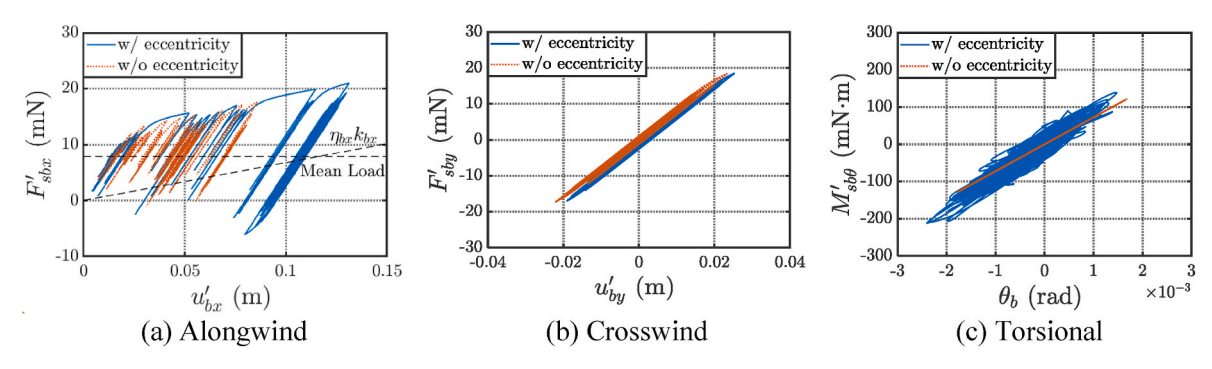


Fig. 9. Restoring force-deformation relation of base isolation system ($U_H=40~\mathrm{m/s}$).

generalized mass.

Consider the case of eccentricity: $e_{xi} = e_{yi} = e_{bx} = e_{by} = -0.4r$. The modal properties of base-isolated building with initial stiffness of isolation system are listed in Table 5. The damping matrix of the upper building is the same as that of fixed-base building with eccentricity. As compared to those of the fixed-base building with eccentricity, the base isolation leads to 7% reduction in three fundamental modal frequencies. Fig. 7 shows the coupled mode shapes of three fundamental modes.

The accuracy of the reduced-order model of upper building is also examined. It is observed that the reduced 4DOFs model in each direction can accurately represent the modal properties of the first two modes in each direction (even first three modes in each direction) of base-isolated building. The reduced model with 4DOFs in each direction, i.e., a total of 12 DOFs, is used in the response analysis of this study.

0.5

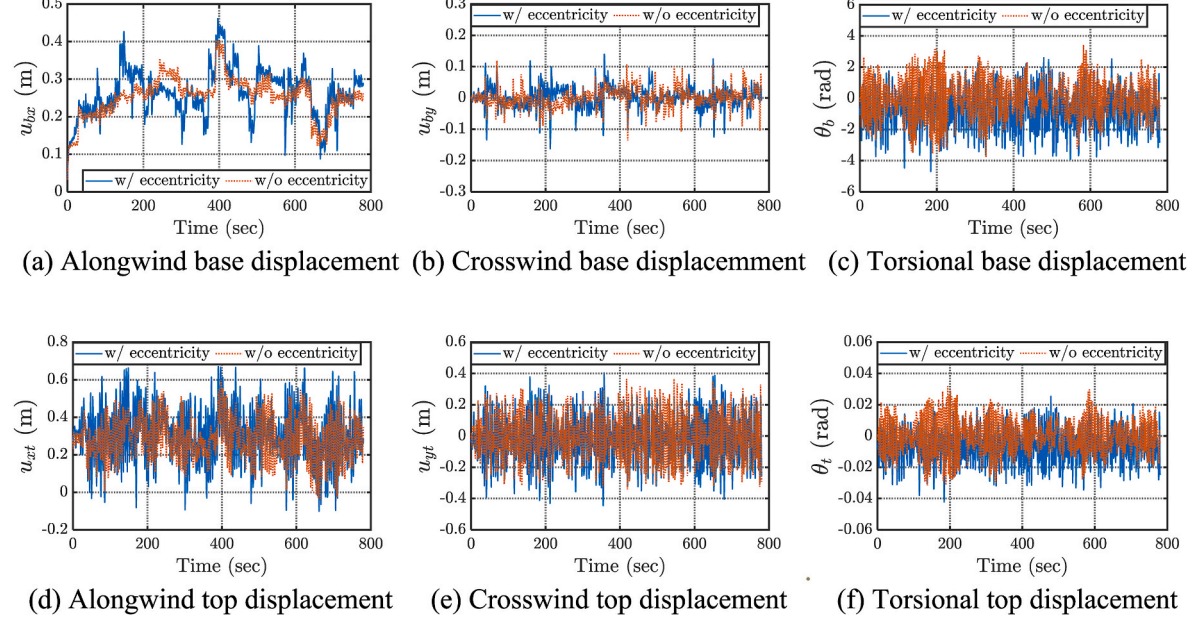


Fig. 10. Time history samples of building response ($U_H = 60 \text{ m/s}$).

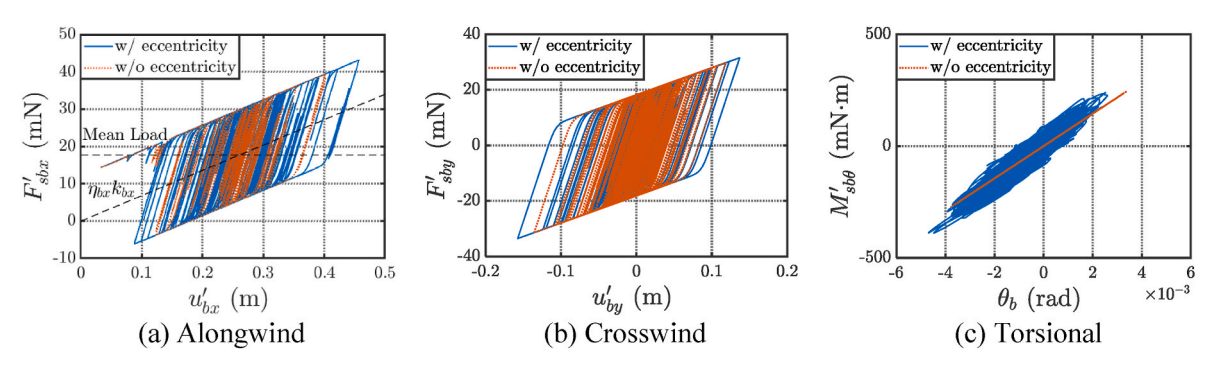


Fig. 11. Restoring force-deformation relation of base isolation system ($U_H = 60 \text{ m/s}$).

Table 6 STDs and correlation coefficients of responses for fixed-base building with different eccentricities ($U_H = 60 \text{ m/s}$).

Response		STD			Correlation coefficient			
		σ_{χ}	$\sigma_{\rm y}$	$\sigma_{ heta}$	ρ_{xy}	$ ho_{{ m x} heta}$	$ ho_{y heta}$	
Top displacement (m, or rad)	Case 0	0.142	0.201	0.0101	0	0	0	
	Case 1	0.236	0.215	0.0145	0.01	-0.41	0.70	
	Case 2				0.01	0.41	-0.70	
	Case 3				-0.01	0.41	0.70	
	Case 4				-0.01	-0.41	-0.70	
Top acceleration (m/s ² , or rad/s ²)	Case 0	0.235	0.504	0.0375	0	0	0	
	Case 1	0.391	0.461	0.0401	0.25	0.04	0.29	
	Case 2				0.25	-0.03	-0.29	
	Case 3				-0.25	-0.04	0.29	
	Case 4				-0.25	0.03	-0.29	

5. Characteristics of building response

5.1. Response time history

The building response history analysis (RHA) under different mean wind speeds is carried out using Runge-Kutta method. The mean wind speed is along positive *x*-axis. The wind speed at building top varies from 20 to 60 m/s. The translational hysteretic restoring forces of base isolation system are represented by uniaxial force model. The influence

of biaxial interaction of hysteretic restoring forces will be discussed in the later part of this study. The wind load time histories are simulated using spectral representation method (Shinozuka and Jan 1972; Chen and Kareem, 2005c). For comparison purpose, both base-isolated buildings with and without eccentricity of C.R. are considered. The time step is 0.04 s and duration 13 min for each sample, where the first 3 min was removed for eliminating transient effect. There is a total of 100 samples simulated for each wind speed and the response statistics are calculated by ensemble average. The responses of interest are building

Table 7 STDs and correlation coefficients of responses for base-isolated building with different eccentricities ($U_H = 60 \text{ m/s}$).

Response		STD			Correlation of	Correlation coefficient			
		σ_{x}	σ_{y}	$\sigma_{ heta}$	ρ_{xy}	$\rho_{x\theta}$	$\rho_{y\theta}$		
Base displacement (m, or rad)	Case 0	0.0392	0.0308	0.00123	0.02	0.01	-0.01		
	Case 1	0.0554	0.0336	0.00119	-0.03	-0.17	0.42		
	Case 2				-0.03	0.17	-0.42		
	Case 3				0.01	0.17	0.44		
	Case 4				0.03	-0.17	-0.44		
Top displacement (m, or rad)	Case 0	0.113	0.132	0.0109	0.01	0.00	-0.01		
	Case 1	0.147	0.149	0.0103	-0.04	-0.36	0.66		
	Case 2				-0.04	0.36	-0.66		
	Case 3				0.05	0.37	0.66		
	Case 4				0.04	-0.36	-0.67		
Top acceleration (m/s ² , or rad/s ²)	Case 0	0.185	0.366	0.0400	0.01	0.00	0.00		
	Case 1	0.274	0.341	0.0333	0.19	0.08	0.22		
	Case 2				0.19	-0.08	-0.22		
	Case 3				-0.18	0.08	0.24		
	Case 4				-0.18	0.08	-0.24		

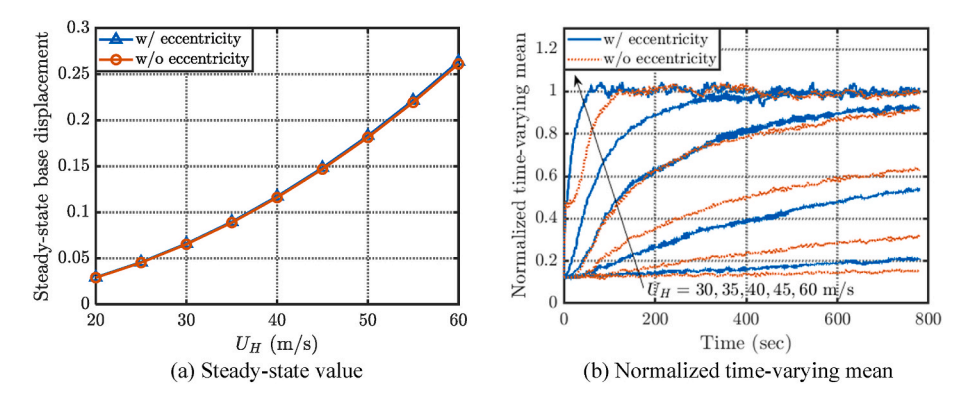


Fig. 12. Time-varying mean base displacement in alongwind direction.

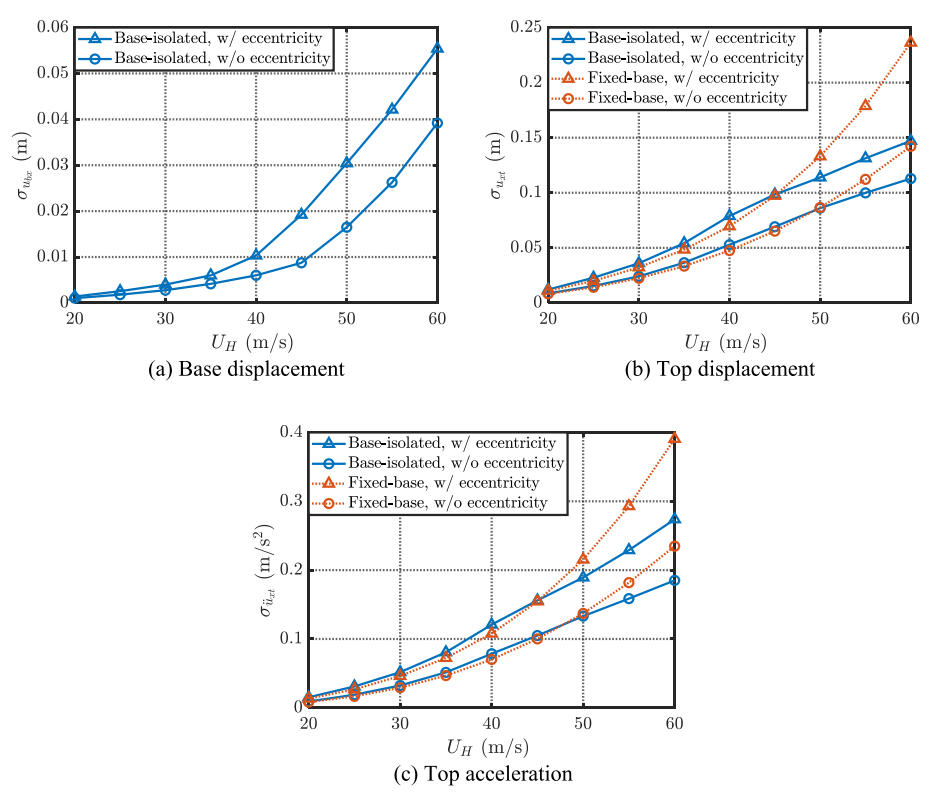


Fig. 13. STDs of alongwind responses.

top displacement and acceleration as well as base displacement of base-isolation system. The upper building displacement is relative to base displacement, and the upper building acceleration is absolute acceleration relative to ground. The building base bending moments and torque have similar response characteristics as the building top displacement thus will not be discussed. Furthermore, the response statistics of fixed-base buildings are also analyzed using spectral method for comparison.

The time histories of responses of base-isolated building with and without eccentricity at $U_H=40~\text{m/s}$ are shown in Fig. 8. These responses include base displacements and building top displacements in three directions. The hysteretic loops of restoring forces (torque) and base displacements at C.R. are shown in Fig. 9. Figs. 10 and 11 are the results at $U_H=60~\text{m/s}$. Tables 6 and 7 summarize the STDs of 3D responses and their correlation coefficients of fixed-base and based-isolated buildings with and without eccentricity at $U_H=60~\text{m/s}$.

The base displacements in both alongwind and crosswind directions exceed the yielding displacements at both wind speeds. The yielding causes the alongwind base displacement drift in the mean wind load direction in terms of time-varying mean around which the fluctuating component is observed. The drift continues until reaching the steadystate level, which is determined by the static wind force and postyielding stiffness. A larger fluctuating response results in more frequent yielding thus faster growth of time-varying mean displacement. It rapidly reaches steady-state displacement at $U_H = 60 \text{ m/s}$ as compared to that at $U_H = 40$ m/s. For the building without eccentricity, the timevarying mean displacement is only observed in alongwind direction. The steady-state base displacement is 0.116 m and 0.261 m at $U_H = 40$ and 60 m/s, respectively. For buildings with eccentricity, the alongwind static wind load leads to 3D displacements with dominant alongwind component. At $U_H=60$ m/s, the alongwind, crosswind and torsional displacements are 0.264 m, -0.0026 m and -0.0458 deg. The timevarying mean displacement of the building with eccentricity growths faster than that without eccentricity.

5.2. Time-varying mean displacement

Fig. 12(a) displays the steady-steady alongwind base displacement at different mean wind speed for buildings with and without eccentricity, which is determined by static analysis under static wind load using post-yielding stiffness. The eccentricity also leads to slight displacements in crosswind and torsional directions. The steady-state displacement is proportional to wind speed squared. Fig. 12(b) shows the time-varying alongwind base displacement normalized by the corresponding steady-state mean value, which is estimated from ensemble average of 100 simulated time history samples. The time-varying mean displacement grows faster at higher wind speed due to larger fluctuating response and more frequent yielding, which corresponds to a higher hysteretic damping. The eccentricity leads to faster growth of time-varying mean displacement resulted from a higher hysteretic damping.

5.3. Statistics of fluctuating response

The fluctuating building response with mean load is the same as that without mean load since the hysteretic loop with non-zero mean load and response is simply moved to a new position without changing its shape (e.g., Roberts and Spanos, 2003; Feng and Chen, 2019a). The response statistics of fluctuating response can be calculated from the response without consideration of the mean load.

Figs. $13\sim15$ show the STDs of responses at different wind speeds. Figs. $16\sim18$ portray the peak factors. Fig. 19 shows the kurtoses of alongwind and crosswind base displacements. It is evident that the responses of base-isolated building with and without eccentricity are higher than those of the fixed-base building at lower wind speeds due to reduction of natural frequency by base isolation system. On the other hand, the responses of base-isolated building are lower at higher wind speeds, which is due to additional hysteretic damping caused by yielding of base isolation system. The torsional response of base-isolated building without eccentricity remains linear elastic and is slightly higher than that of fixed-base building. The damping ratio of base isolation system ξ_b

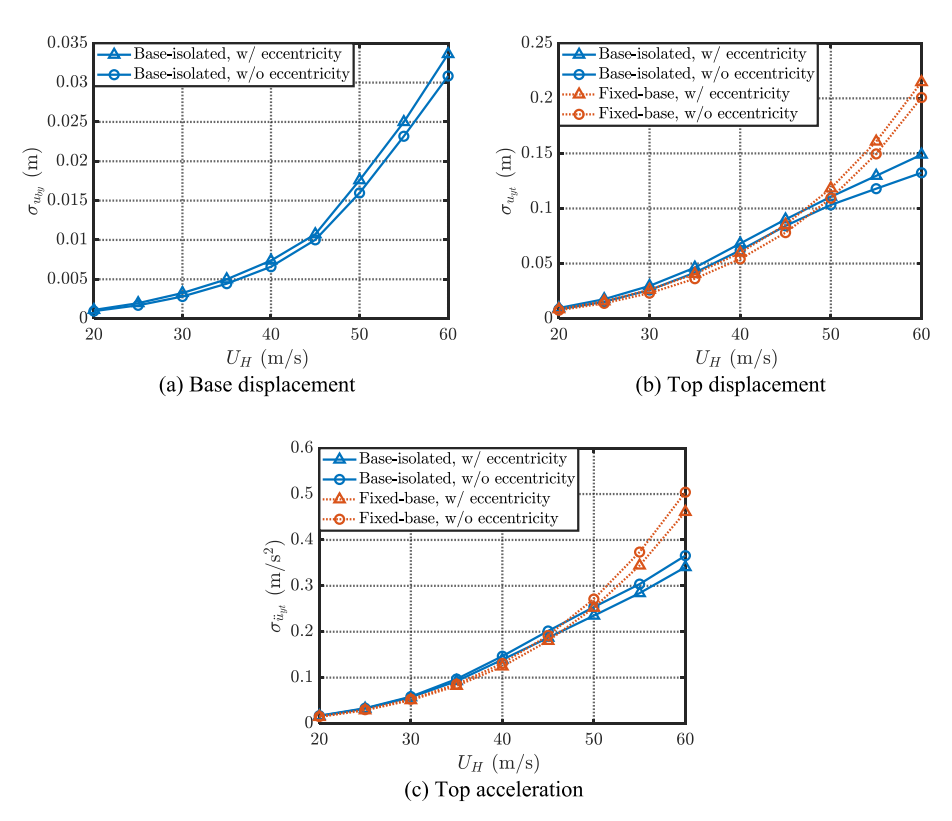


Fig. 14. STDs of crosswind responses.

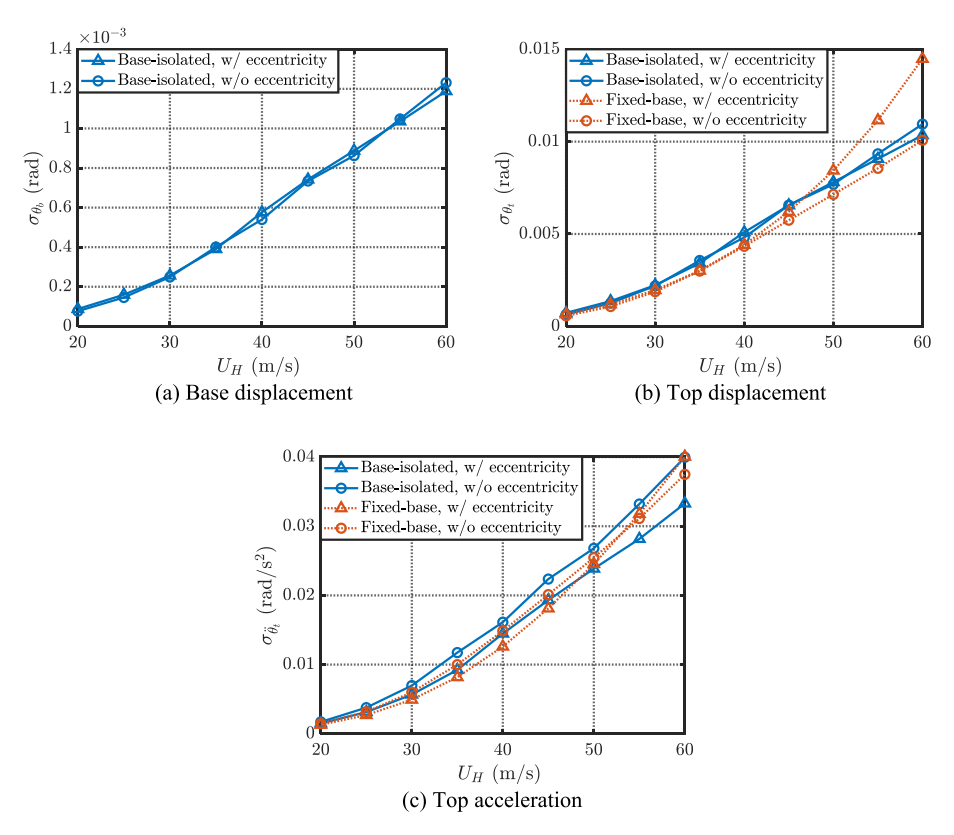


Fig. 15. STDs of torsional responses.

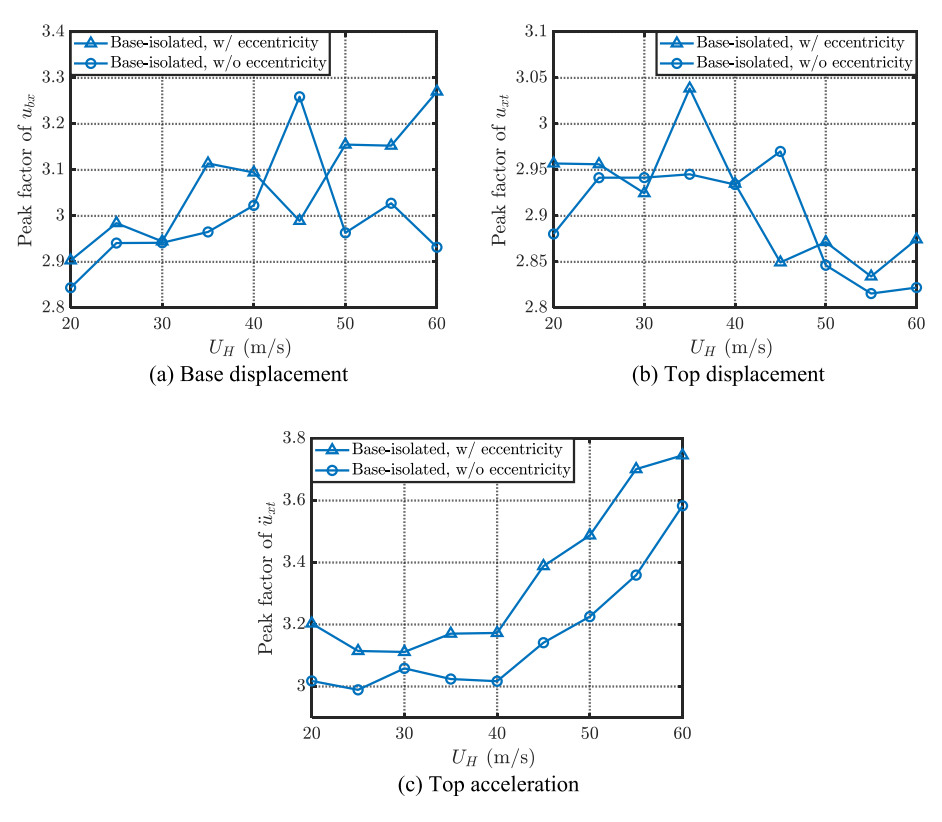


Fig. 16. Peak factors of alongwind responses.

is not included in this analysis. Feng and Chen (2019a) have investigated the influence of damping ratio ξ_b on uncoupled building responses. An increase in ξ_b leads to decrease in the base displacement and building

top acceleration, and the reductions are more noticeable when ξ_b is lower. The building top displacement decreases at lower wind speeds, where the base displacement is elastic. However, it is almost not affected

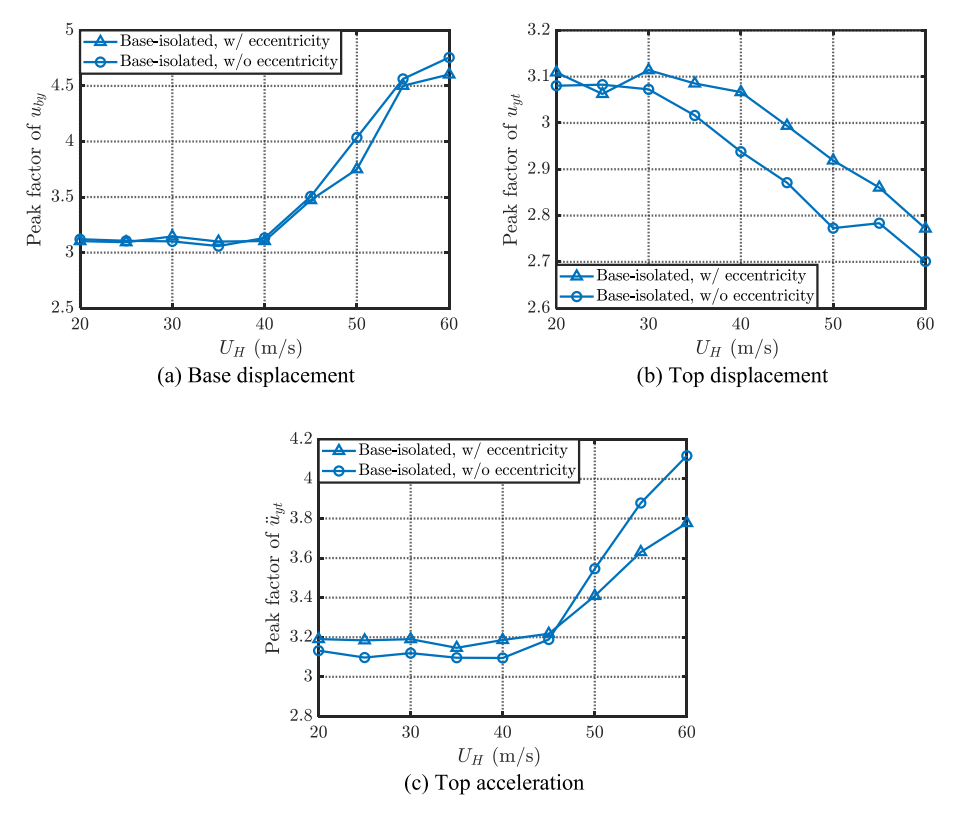


Fig. 17. Peak factors of crosswind responses.

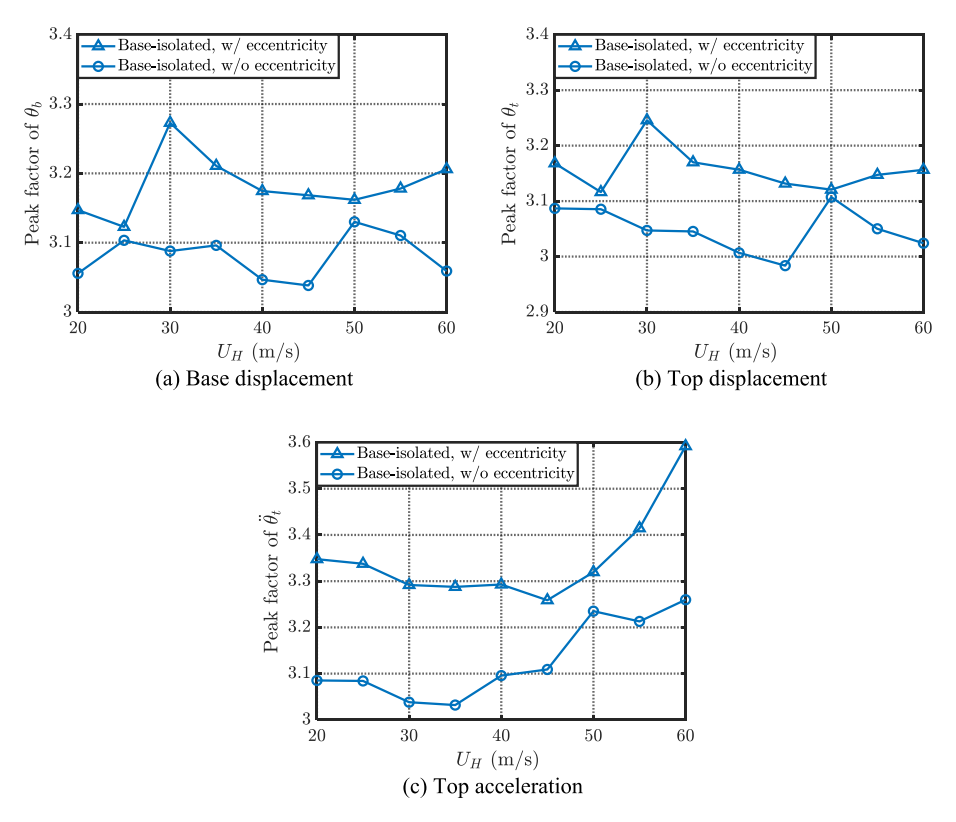
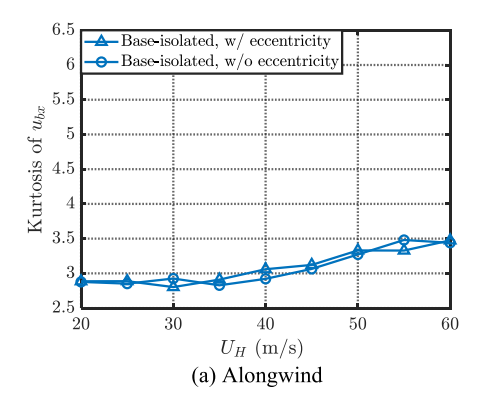


Fig. 18. Peak factors of torsional responses.

by damping ratio ξ_b at higher wind speeds, where the base displacement is inelastic and additional hysteretic damping is resulted that reduces the influence of damping ratio ξ_b .

It is observed that in the case of base-isolated building without ec-

centricity at $U_H = 60$ m/s, the base isolation leads to 20% and 21% decreases, 34% and 27% decreases, 8% and 7% increases in the STDs of building top displacements and accelerations in alongwind, crosswind and torsional directions, respectively. The normalized accumulated



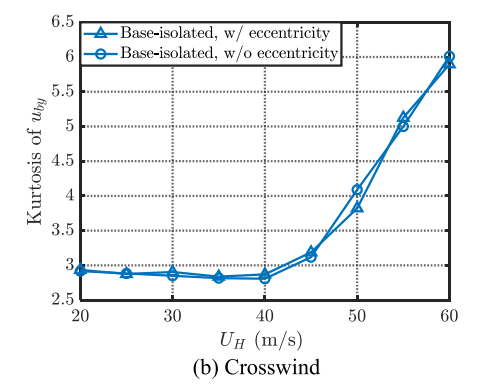


Fig. 19. Kurtoses of base displacements.

dissipated hysteretic energy levels in the duration of 780 s associated with alongwind and crosswind responses are 44 and 163 calculated using Eq. (4). The crosswind response of base has more yielding than the alongwind response. The increase in hysteretic damping resulted from yielding in both alongwind and crosswind directions, particularly from the higher level of yielding in crosswind direction, reduces the ratio of these two responses. The STD ratio of crosswind to alongwind building top displacement is reduced to 1.17 from 1.42.

For the base-isolated building with eccentricity at $U_H=60~\rm m/s$, the base isolation leads to 38% and 30%, 31% and 26%, 29% and 17% decreases in the STDs of building top displacements and accelerations in alongwind, crosswind and torsional directions, respectively. The reduction of torsional displacement is resulted from the reduction of coupled alongwind and crosswind responses. The normalized dissipated hysteretic energy levels in the duration of 780 s in two directions is 158 and 154, respectively. While the STD of alongwind base displacement is much greater than that of crosswind displacement, the dissipated hysteric energy is quite close, which is related to different power spectral characters of both responses. Obviously, the base isolation system is more effective for buildings with eccentricity.

From the perspective of the influence of eccentricity on building response, it is observed that, in the case of fixed-base building, the eccentricity leads to 66% increase in the STDs of alongwind building top displacement and acceleration. The crosswind top displacement and acceleration are increased by 7% and decreased by 9%, respectively. The torsional building top displacement and acceleration are increased by 44% and 7%, respectively.

A simple physical explanation of the effect of eccentricity on building response may be given from the point of view of static response. Due to the eccentricity of C.R., both alongwind and crosswind loads not only lead to alongwind and crosswind responses respectively, but also cause torsional response around the C.R., which results in additional displacements in both alongwind and crosswind directions. This additional displacement in crosswind direction is relatively less noticeable as crosswind response caused by crosswind load is larger than the alongwind response. The effect of eccentricity on dynamic response is more complicated due to additional effects of three-dimensional inertial and damping forces.

In the case of base-isolated building, the eccentricity leads to 30% and 48% increases in the STD of alongwind building top displacement and acceleration, 13% increase and 7% decrease in crosswind top displacement and acceleration, 6% and 17% decreases in torsional building top displacement and acceleration. The STDs of alongwind and crosswind base displacements are increased by 41% and 9%, respectively, while torsional displacement is only decreased by 3%. The decrease in the ratio of crosswind to alongwind displacements of base-isolated building leads to less increase in alongwind displacement due to eccentricity. The yielding further reduces the alongwind top displacement. As a result, the eccentricity has less effect on inelastic

response of base-isolated building as compared to fixed-base building.

At $U_H=40\,\mathrm{m/s}$ the yielding levels of alongwind and crosswind base displacements are lower than those at $U_H=60\,\mathrm{m/s}$. In the case of base-isolated building without eccentricity, the normalized dissipated hysteretic energy in the duration of 780 s associated with alongwind and crosswind displacements is 0.91 and 0.70, respectively. The base isolation leads to 11% and 12%, 14% and 12%, 11% and 8% increases in STDs of building top displacements and accelerations in alongwind, crosswind and torsional directions, respectively. On the other hand, for the building with eccentricity, the base isolation leads to 13% and 12%, 14% and 12%, 16% and 15% increase in these responses. The base isolation has similar effect on elastic responses of buildings with and without eccentricity.

Regarding the influence of the eccentricity at $U_H=40~\rm m/s$, it leads to 46% and 53% increase in the STDs of alongwind building top displacement and acceleration in the case of fixed-base building. For the base-isolated building, the eccentricity leads to 49% and 54% increases in the STDs of alongwind building top displacement and acceleration, 72% increase in alongwind base displacement. The eccentricity has similar effect on elastic responses of fixed-base and base-isolated building. Obviously, the increase in the yielding level leads to decrease in the effect of eccentricity, increase in the effect of base isolation.

The crosswind base displacement of base-isolated building at higher wind speeds shows apparent softening non-Gaussian distribution with a kurtosis greater than 3. The peak factor is higher than the Davenport peak factor (Davenport, 1964) of a Gaussian process. The alongwind base displacement shows less apparent softening non-Gaussian character at higher wind speeds. The building top displacement is close to a Gaussian process, while slightly hardening non-Gaussian character with reduced peak factors are observed at higher wind speeds. The building top absolute acceleration shows softening non-Gaussian character at higher wind speeds due to the contribution of non-Gaussian base acceleration. The torsional response is almost Gaussian and less affected by yielding of base. The peak factors of torsional responses are almost independent of wind speed and are close to Gaussian peak factor in the range of 3.0-3.3 for base displacement and top displacement, and in the range of 3.0-3.6 for top acceleration. The kurtoses of torsional responses are in the range of 2.7-2.9. The eccentricity also shows little influence on the non-Gaussian character of alongwind base displacement.

5.4. Correlations of responses

The eccentricity affects not only the magnitudes of 3D responses but also their correlations. Tables 6 and 7 summarize the STDs and correlation coefficients of building top displacements and accelerations at the center at $U_H = 60$ m/s for both fixed-base and base-isolated buildings. To investigate the influence of location of eccentricity, the following cases are compared: Case 0: $e_x/r = e_y/r = 0$; Case 1: $e_x/r = e_y/r = -1$

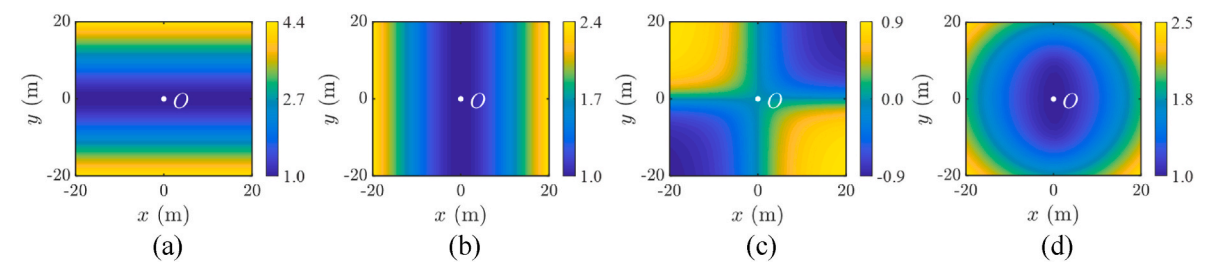


Fig. 20. Variations of response statistics of base-isolated building without eccentricity. (a) STD of alongwind acceleration; (b) STD of crosswind acceleration; (c) Correlation coefficient; (d) Mean extreme of total acceleration.

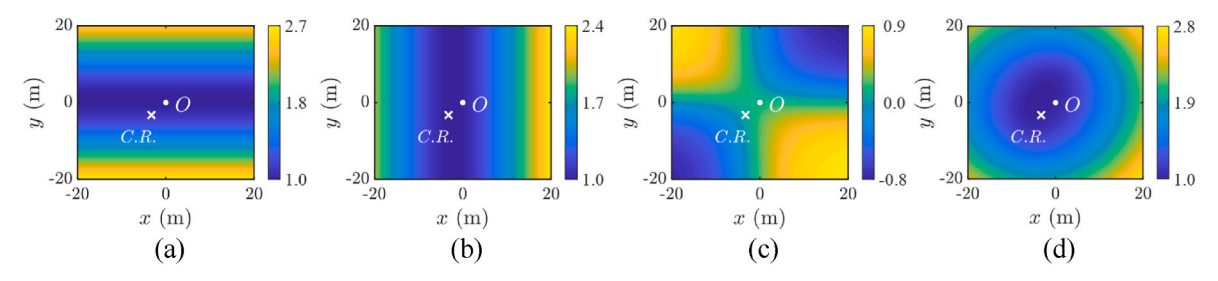


Fig. 21. Variations of response statistics of base-isolated building with eccentricity (Case 1). (a) STD of alongwind acceleration; (b) STD of crosswind acceleration; (c) Correlation coefficient; (d) Mean extreme of total acceleration.

0.4; Case 2: $e_x/r = e_y/r = 0.4$; Case 3: $e_x/r = -0.4$, $e_y/r = 0.4$; Case 4: $e_x/r = 0.4$, $e_y/r = -0.4$, where Case 0 is the case without eccentricity, and Case 1 is case with eccentricity discussed previously. The base isolation system has same eccentricity of upper building.

The STDs of building responses at the floor center remain the same for different cases of eccentricity considered. The correlation coefficients are also same while there are differences in signs. The correlations of responses in three directions directly affects statistics of their combined response. For instance, the STDs of alongwind and crosswind accelerations and their correlation coefficient at location (x, y) of the building top are estimated from the statistics of accelerations at the

origin (center) O as

$$\sigma_{\ddot{u}_{x}}(x,y) = \sqrt{\sigma_{\ddot{u}_{x}}^{2} + (y/r)^{2}\sigma_{\ddot{u}_{\theta}}^{2} - 2(y/r)\sigma_{\ddot{u}_{x}}\sigma_{\ddot{u}_{\theta}}\rho_{\ddot{u}_{x}\ddot{u}_{\theta}}}$$
(24a)

$$\sigma_{\ddot{u}_{y}}(x,y) = \sqrt{\sigma_{\ddot{u}_{y}}^{2} + (x/r)^{2} \sigma_{\ddot{u}_{\theta}}^{2} + 2(x/r) \sigma_{\ddot{u}_{y}} \sigma_{\ddot{u}_{\theta}} \rho_{\ddot{u}_{y}\ddot{u}_{\theta}}}$$
(24b)

$$\rho_{\vec{u}_x\vec{u}_y}(x,y) = \frac{\sigma_{\vec{u}_x}\sigma_{\vec{u}_y}\rho_{\vec{u}_x\vec{u}_y} + (x/r)\sigma_{\vec{u}_x}\sigma_{\vec{u}_\theta}\rho_{\vec{u}_x\vec{u}_\theta} - (y/r)\sigma_{\vec{u}_y}\sigma_{\vec{u}_\theta}\rho_{\vec{u}_y\vec{u}_\theta} - (xy/r^2)\sigma_{\vec{u}_\theta}^2}{\sigma_{\vec{u}_x}(x,y)\sigma_{\vec{u}_y}(x,y)}$$
(24c)

where $\sigma_{\ddot{u}_x}$, $\sigma_{\ddot{u}_y}$, $\sigma_{\ddot{u}_\theta}$, $\rho_{\ddot{u}_x\ddot{u}_y}$, $\rho_{\ddot{u}_x\ddot{u}_\theta}$ and $\rho_{\ddot{u}_y\ddot{u}_\theta}$ are the STDs and correlation co-

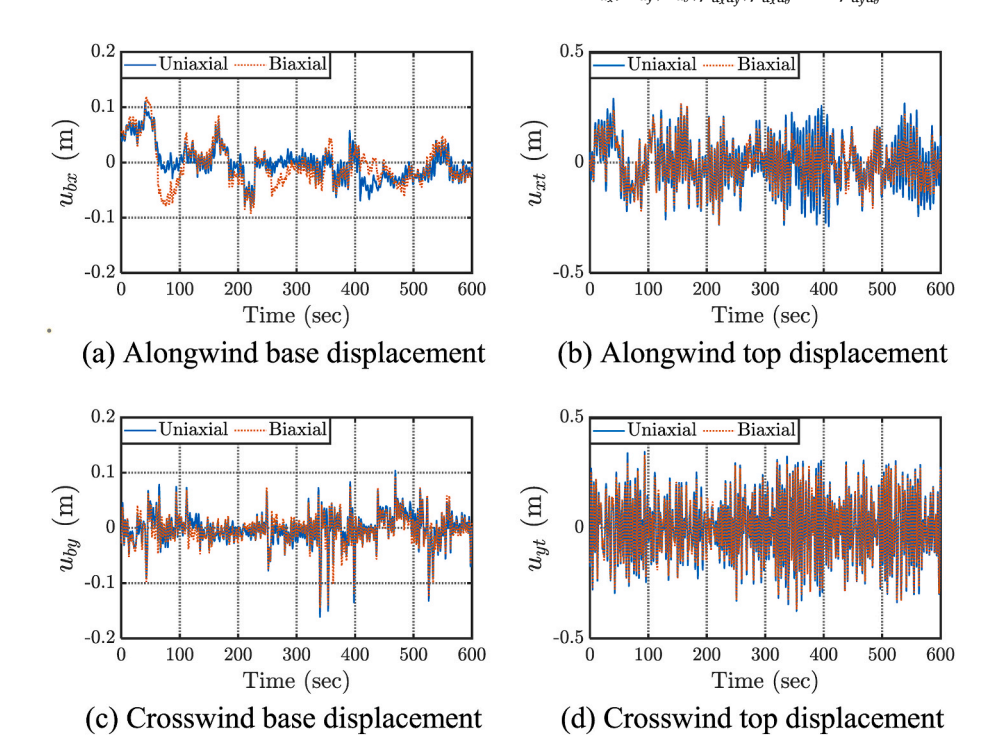


Fig. 22. Time history samples of base and top displacements of base-isolated building without eccentricity ($U_H = 60 \text{ m/s}$).

Table 8 STDs and correlation coefficients of responses for base-isolated building with biaxial hysteretic force model ($U_H = 60 \text{ m/s}$).

Response		STD			Correlation	Correlation coefficient		
		σ_{x}	$\sigma_{ m y}$	$\sigma_{ heta}$	ρ_{xy}	$ ho_{x heta}$	$\rho_{y\theta}$	
Base displacement (m, or rad)	w/o eccentricity	0.0452	0.0312	0.00123	0.01	0.01	-0.01	
	w/eccentricity	0.0558	0.0346	0.00113	0.01	-0.18	0.42	
Top displacement (m, or rad)	w/o eccentricity	0.0994	0.125	0.0109	0.01	0.00	-0.01	
	w/eccentricity	0.136	0.138	0.00980	-0.11	-0.40	0.66	
Top acceleration (m/s ² , or rad/s ²)	w/o eccentricity	0.167	0.344	0.0400	0.00	0.00	0.00	
	w/eccentricity	0.252	0.315	0.0310	0.17	0.08	0.20	

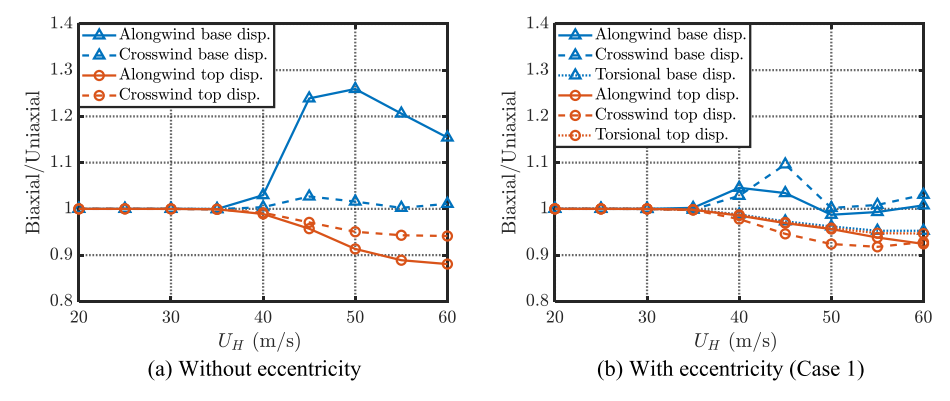


Fig. 23. Effect of biaxial interaction on responses of base-isolated building.

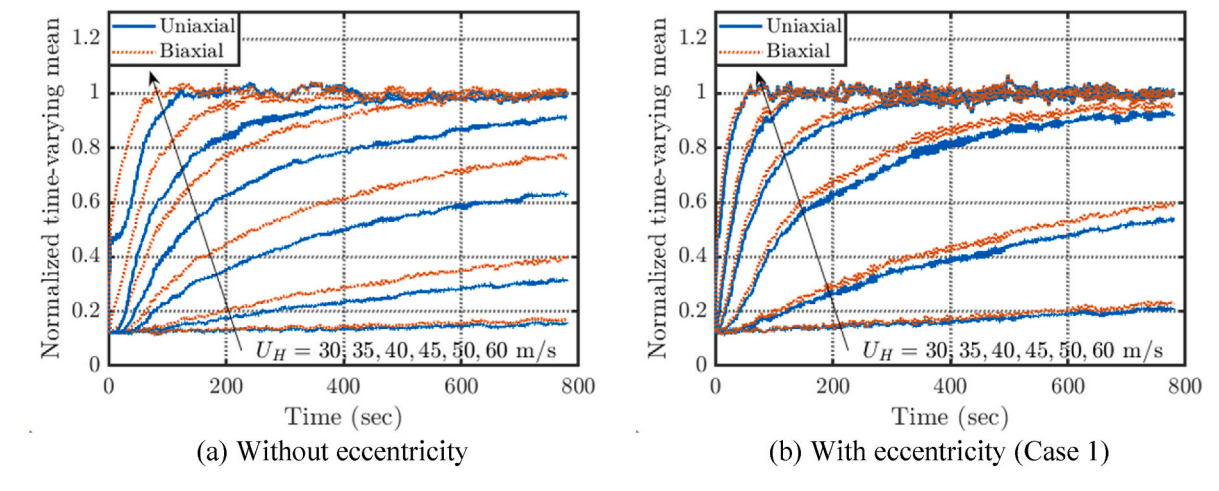


Fig. 24. Effect of biaxial interaction on normalized time-varying mean alongwind base displacement of base-isolated building.

efficients of accelerations at the origin.

Fig. 20(a) and (b) show STDs of alongwind and crosswind accelerations at different locations of top of base-isolated building without eccentricity, i.e., Case 0, normalized by the STDs at the center, respectively. According to Eq. (24a), the STD of alongwind acceleration increases with the distance in y direction from the center due to contribution of torsional response and is symmetric about x axis. The alongwind accelerations at four conners are 4.4 times that at the center due to significant contribution of torsional response. Similarly, the STD of crosswind acceleration increases with the distance in x direction and is symmetric about y axis. The crosswind accelerations at four conners are 2.4 times that at the center. Fig. 20(c) shows their correlation coefficient. According to Eq. (24c), due to the term $-(xy/r^2)\sigma_{ii.}^2$, the correlation coefficient is positive in Quadrants II and IV, and negative in Quadrants I and III. At four conners, the correlation coefficients are \pm 0.88. The mean extreme of the total absolute acceleration $\ddot{u}(t) =$ $\sqrt{\ddot{u}_x^2(t) + \ddot{u}_y^2(t)}$ is estimated using response time histories, which is 1.58

 m/s^2 at the center. Fig. 20(d) shows the distribution of mean extreme of the absolute acceleration normalized by that at the center. The extreme acceleration at four conners is 2.5 times the acceleration at the center.

Fig. 21 shows the results of the base-isolated building with eccentricity, i.e., Case 1. The alongwind accelerations at right upper and lower conners are 2.6 and 2.7 times that at the center. These ratios are higher than the case of fixed-base building due to more reduction in alongwind acceleration over the torsional acceleration. The crosswind accelerations at these two conners are 2.4 times that at the center. The correlation coefficients of alongwind and crosswind accelerations at these two conners are -0.81 and 0.88. The mean extreme absolute accelerations at these two corners are 2.7 and 2.8 times that at center. The mean extreme absolute acceleration at the center is $1.46~\mathrm{m/s^2}$.

6. Biaxial interaction of base hysteretic restoring forces

The influence of biaxial interaction of hysteretic restoring forces of

Table 9STDs and correlation coefficients of responses for fixed-base building.

Response		STD			Correlation coefficient		
		σ_{x}	$\sigma_{ m y}$	$\sigma_{ heta}$	ρ_{xy}	$ ho_{ ext{x} heta}$	$\rho_{y\theta}$
Top displacement (m, or rad)	w/o eccentricity	0.383	0.0866	0.0101	0.00	0.00	0.00
	w/eccentricity	0.421	0.200	0.0212	-0.67	-0.87	0.82
Top acceleration (m/s ² , or rad/s ²)	w/o eccentricity	0.672	0.197	0.0375	0.00	0.00	0.00
- , , , , , , ,	w/eccentricity	0.635	0.373	0.0442	-0.47	-0.53	0.38

 $(U_H = 60 \text{ m/s}, \text{ wind direction of } 90 \text{ deg}).$

Table 10 STDs and correlation coefficients of responses for base-isolated building with uniaxial model ($U_H = 60 \text{ m/s}$, wind direction of 90 deg).

Response		STD			Correlation coefficient		
		σ_x	σ_y	$\sigma_{ heta}$	ρ_{xy}	$ ho_{x heta}$	$ ho_{y heta}$
Base displacement (m, or rad)	w/o eccentricity	0.0776	0.0164	0.00125	-0.01	-0.01	0.00
· · · · · · · · · · · · · · · · · · ·	w/eccentricity	0.0884	0.0243	0.00129	-0.13	-0.42	0.39
Top displacement (m, or rad)	w/o eccentricity	0.177	0.0893	0.0111	0.00	-0.01	0.00
	w/eccentricity	0.209	0.117	0.0112	-0.40	-0.69	0.65
Top acceleration (m/s ² , or rad/s ²)	w/o eccentricity	0.425	0.200	0.0406	0.00	0.00	0.00
	w/eccentricity	0.424	0.287	0.0336	-0.27	-0.35	0.19

Table 11STDs and correlation coefficients of responses for base-isolated building with biaxial model.

Response		STD			Correlation coefficient		
		σ_{x}	σ_y	$\sigma_{ heta}$	ρ_{xy}	$ ho_{{ m x} heta}$	$\rho_{y\theta}$
Base displacement (m, or rad)	w/o eccentricity	0.0782	0.0338	0.00125	0.01	-0.01	0.00
	w/eccentricity	0.0872	0.0397	0.00120	-0.25	-0.49	0.31
Top displacement (m, or rad)	w/o eccentricity	0.175	0.0627	0.0111	0.00	-0.01	0.00
	w/eccentricity	0.203	0.100	0.0102	-0.49	-0.74	0.67
Top acceleration (m/s ² , or rad/s ²)	w/o eccentricity	0.419	0.142	0.0406	0.00	0.00	0.00
	w/eccentricity	0.406	0.244	0.0310	-0.38	-0.38	0.19

 $(U_H = 60 \text{ m/s}, \text{ wind direction of } 90 \text{ deg}).$

base-isolation system on building responses is investigated through the comparison of the results under uniaxial restoring force model. Fig. 22 shows a comparison of time history samples at $U_H=60~\rm m/s$ under uniaxial and biaxial hysteretic restoring force models for the based-isolated building without eccentricity. Table 8 summarizes the response STDs and correlation coefficients of the base-isolated building with biaxial interaction. Both building with and without eccentricities are included. The comparison of these results with those shown in Table 7 sheds insight on the effect of biaxial interaction on the STD of building response. Fig. 23 shows the ratio of STD of response with biaxial model over that with uniaxial model at different wind speed. Fig. 24 displays the time-varying mean alongwind base displacement.

In the case of building without eccentricity, the biaxial interaction leads to 15% increase of alongwind base displacement at $U_H=60~\rm m/s$. The response power spectral analysis indicated that this increase is a result of 15% increase in low-frequency component with a frequency less than 0.1 Hz and 5% decrease in resonant component around the first modal frequency. The increase in the low-frequency alongwind base displacement does not affect upper building relative displacement and acceleration as the frequency is much lower than the modal frequency of the upper building. The STDs of alongwind top displacement and acceleration are reduced by 12% and 10% attributed to the decrease in resonant alongwind base displacement. The crosswind base displacement is almost not affected by biaxial interaction. The biaxial interaction has no influence on torsional response. The biaxal interaction leads to faster growth in time-varying mean alongwind base displacement, while the steady-state value is not affected.

In the case of base-isolated building with eccentricity, the alongwind response is amplified due to eccentricity. Both responses have similar level of yielding, which leads to less influence of biaxial interaction on response STD and time-varying mean base displacement. The reduction of building top displacement due to biaxial interaction is also reduced.

7. Wind direction of 90 degrees

The influence of eccentricity, base isolation and biaxial interaction of hysteretic base restoring forces are affected by ratio of alongwind and crosswind responses. To further explore these influences, now wind direction of 90° is considered, where the positive alongwind and crosswind directions are along the positive y- and negative x-axis, respectively.

Tables 9 \sim 11 summary the STDs and correlation coefficients of responses at the center at $U_H=60$ m/s for fixed-base and base-isolated building with uniaxial and biaxial hysteretic forces. At wind direction of 90° , the crosswind response is much larger than alongwind response as compared to the previous case study of zero wind direction. This is due to the lower building stiffness in crosswind direction. The STD ratio of crosswind to alongwind building top displacements is 4.42. A larger amplification effect of eccentricity on lower alongwind response is expected. The eccentricity leads to 131% increase in the STD of alongwind top displacements as compared to 66% increase in the case of zero wind direction. It is also noted that the responses become more correlated. For the base-isolated building with uniaxial hysteric forces, the yielding of crosswind base displacement leads to 54% decrease in crosswind

building top displacement, while the alongwind building top displacement remains unchanged. The normalized accumulated dissipated hysteretic energy during duration of 780s in alongwind and crosswind directions is 6 and 783 for building without eccentricity. The STD ratio of crosswind to alongwind building top displacements is 1.98. The eccentricity leads to 31% increase in the STD of alongwind top displacement with 48% increase in the alongwind base displacement, which correspond to 30% and 41% in the case of zero wind direction. The base isolation results in 42% and 50% reduction in alongwind and crosswind building top displacement. The normalized dissipated hysteretic energy during duration of 780s in both directions is 17 and 894.

The biaxial interaction of hysteretic forces of base isolation system leads to increase of alongwind base displacement, primarily the low-frequency component, but slight decrease in resonant component of alongwind base displacement. It contributes to 30% and 15% reduction of top displacements of building without and with eccentricity. The eccentricity leads to 17% increase in alongwind base displacement, 59% increase in alongwind top displacements. The biaxial interaction reduces the effect of eccentricity on base displacements but increases the effect on top displacement.

8. Conclusions

The modal analysis of based-isolated building with eccentricity demonstrated that the upper building displacements relative to base isolation slab can be well represented in small number of lower modal displacements using the modal shapes of fixed-base building. It permits use of reduced-order model of base-isolated building to greatly improve the efficiency of dynamic response analysis.

The eccentricity leads to coupled alongwind, crosswind and torsional building responses. The eccentricity changes not only the magnitudes of responses but also their correlations, subsequently affects the statistics of combined responses at different floor locations. The crosswind response is generally larger than alongwind response for the building without eccentricity. The eccentricity amplifies the alongwind response but shows relatively less influence on crosswind and torsional responses.

The linear elastic response of base-isolated building with eccentricity has similar characteristics as the fixed-base building. At higher wind speeds, the base isolation system shows inelastic response in both alongwind and crosswind directions. The yielding causes drift of base displacement primarily in alongwind direction while very low levels of drifts in crosswind and torsional directions are observed due to the eccentricity of center of resistance. The drift continues until reaching the steady-state value, which is determined by the static wind load and post-

yielding building stiffness. The yielding introduces additional hysteretic damping and reduces the dynamic response. The inelastic base displacement shows softening non-Gaussian distribution with an increased peak factor. The torsional base displacement remains linear elastic. The upper building response relative to base is close to a Gaussian process.

The influence of eccentricity is less on the inelastic response of based-isolated building as compared to the fixed-base building. The inelastic crosswind response is more reduced due to higher level of yielding. As a result, the ratio of crosswind to alongwind responses reduces which results in less effect of eccentricity. When the amplified alongwind response also exceeds yield displacement, the alongwind response thus the effect of eccentricity is further reduced. The eccentricity results in fast development of time-varying mean displacement. The base isolation is more effective for building with eccentricity as compared to building without eccentricity.

The biaxial interaction of hysteretic forces of base isolation system leads to increase of inelastic alongwind base displacement, primarily the low-frequency component, but decrease in resonant component of alongwind base displacement. The increase in low-frequency alongwind base displacement does not affect the upper building relative response. On the other hand, the decrease in resonant base displacement contributes to the reduction of upper building response. The biaxial effect reduces when the alongwind and crosswind responses are close in magnitude and their yielding levels are low. The biaxial interaction reduces the effect of eccentricity on base displacements but increases the effect on upper building response. The biaxal interaction leads to fast growth in time-varying mean alongwind base displacement, while the steady-state value is not affected.

Declaration of competing interest

The authors declare that they have no known competing financial interests or personal relationships that could have appeared to influence the work reported in this paper.

Data availability

Data will be made available on request.

Acknowledgement

The support for this work provided in part by National Science Foundation (NSF) grant No. CMMI-2153189 is greatly acknowledged.

Appendix. Wind loading model of square-shaped tall building

The STDs of alongwind, crosswind and torsional story force coefficients are

$$\sigma_{C_{P_{sl}}} = 0.09 \left(\frac{z_i}{H}\right)^{0.57} + 0.25$$
 (A1)

$$\sigma_{C_{P_{v_i}}} = 0.33 + 0.03 \left(\frac{z_i}{H}\right) + \left(\frac{z_i}{H}\right)^2 - 1.1 \left(\frac{z_i}{H}\right)^3 \tag{A2}$$

$$\sigma_{C_{P_{dit}}} = 0.072 \tag{A3}$$

The coherence functions of story force coefficients at same direction are given as follows by fitted the wind tunnel data

$$Coh_{xij}(f) = \exp\left(-\sqrt{\left(\frac{0.3\Delta z}{H}\right)^2 + \left(\frac{15f\Delta z}{U_H}\right)^{2.8}}\right)$$
(A4)

$$Coh_{yij}(f) = \exp\left(-\sqrt{\left(\frac{\Delta z}{H}\right)^2 + \left(10\left|\frac{fB}{U_H} - 0.1\right|\left(\frac{\Delta z}{H}\right)\right)^2}\right) when \frac{fB}{U_H} \le 0.1 \ Coh_{yij}(f) = \exp\left(-\sqrt{\left(\frac{\Delta z}{H}\right)^2 + \left(100\left|\frac{fB}{U_H} - 0.1\right|\left(\frac{\Delta z}{H}\right)\right)^{2.5}}\right) when \frac{fB}{U_H} > 0.1 \quad (A5)$$

$$Coh_{\theta ij}(f) = \exp\left(-\sqrt{\left(\frac{0.9\Delta z}{H}\right)^2 + \left(\frac{20f\Delta z}{U_H}\right)^3}\right) \tag{A6}$$

where $\Delta z = |z_i - z_j|$ is the distance between *i*-th and *j*-th stories.

The PSDs of alongwind and crosswind base bending moment coefficients are determined from AIJ recommendations (AIJ, 2004). The PSD of base torque coefficient is given by

$$\frac{fS_{C_{M_{\theta}}}(f)}{\sigma_{C_{M_{\theta}}}^{2}} = \sum_{i=1}^{2} \frac{A_{i}(1+0.6B_{i})B_{i}(f/f_{\theta_{i}})^{C_{i}}}{\pi \left\{ \left[1-(f/f_{\theta_{i}})^{2}\right]^{2}+4B_{i}(f/f_{\theta_{i}})^{2}\right\}}$$
(A7)

where $A_1 = 4.9; A_2 = 0.7; B_1 = 0.5; B_2 = 0.2; C_1 = 1.3; C_2 = 1.4; f_{\theta 1} = 0.05U_H/B; f_{\theta 2} = 0.28U_H/B$.

The cross PSD (CPSD) of crosswind and torsional story force coefficients is modeled as

$$S_{C_{P,i}C_{P,a}}(f) = Coh_{y\theta ij}(f)\sqrt{S_{C_{P,i}}(f)S_{C_{P,a}}(f)}$$
 (A8)

$$Coh_{y\theta ij}(f) = Coh_{y\theta 0}(f)\sqrt{Coh_{yyij}(f)Coh_{\theta\theta ij}(f)}$$
(A9)

$$|Coh_{,\theta0}(f)| = \begin{cases} 0.88, & 0 \le fB/U_H \le 0.1\\ -34(fB/U_H) + 4.28, & 0.1 \le fB/U_H \le 0.12\\ 5.5(fB/U_H) - 0.46, & 0.12 \le fB/U_H \le 0.2\\ 0.64, & 0.2 \le fB/U_H \le 0.4\\ 0.45, & 0.4 \le fB/U_H \le 1.5\\ 0.3, & fB/U_H \ge 1.5 \end{cases}$$
(A10)

$$Coh_{y\theta0}(f)_{Phase} = \begin{cases} 160, & fB/U_H \le 0.1\\ 290 - 1300(fB/U_H) & 0.1 \le fB/U_H \le 0.2\\ 30 & 0.2 \le fB/U_H \le 0.4\\ 330 & 0.4 \le fB/U_H \le 1.5\\ 360 & fB/U_H \ge 1.5 \end{cases}$$
(A11)

References

- AIJ (Architectural Institute of Japan), 2004. AIJ Recommendations for Load of Buildings. AIJ, Tokyo.
- Baber, T.T., 1984. Nonzero mean random vibration of hysteretic systems. J. Eng. Mech. 110 (7), 1036–1049.
- Bhatt, G., 2020. A parametric study on torsionally coupled base-isolated structures. In: Emerging Trends in Civil Engineering. Springer, Singapore, pp. 267–274.
- Chen, X., Kareem, A., 2005a. Coupled dynamic analysis and equivalent static wind loads on buildings with three-dimensional modes. J. Struct. Eng. 131 (7), 1071–1082.
- Chen, X., Kareem, A., 2005b. Dynamic wind effects on buildings with 3D coupled modes: application of high frequency force balance measurements. J. Eng. Mech. 131 (11), 1115–1125
- Chen, X., Kareem, A., 2005c. Proper orthogonal decomposition-based modeling, analysis, and simulation of dynamic wind load effects on structures. J. Eng. Mech. 131 (4), 325–339
- Chopra, A.K., 2017. Dynamics of Structures: Theory and Applications to the Earthquake Engineering, fifth ed. Pearson.
- Davenport, A.G., 1964. Note on the distribution of the largest value of a random function with application to gust loading. Proc. Inst. Civ. Eng. 28 (2), 187–196.
- Feng, C., Chen, X., 2019a. Evaluation and characterization of probabilistic alongwind and crosswind responses of base-isolated tall buildings. J. Eng. Mech. 145 (12), 04019097.
- Feng, C., Chen, X., 2019b. Estimation of inelastic crosswind response of base-isolated tall buildings: performance of statistical linearization approaches. J. Struct. Eng. 145 (12), 04019161.
- Feng, Chen, 2021. Inelastic response of base-isolated tall buildings under nonstationary winds: response history analysis and statistical linearization approach. J. Eng. Mech. 147 (10), 04021067.
- Flay, R.G.J., Yip, D.Y.N., Vickery, B.J., 1999. Wind Induced Dynamic Response of Tall Buildings with Coupled 3D Modes of Vibration. Proceedings of the 10th International Conference on Wind Engineering, Copenhagen, Denmark, pp. 645–652.
- Harvey Jr., P.S., Gavin, H.P., 2014. Truly isotropic biaxial hysteresis with arbitrary knee sharpness. Earthq. Eng. Struct. Dynam. 43 (13), 2051–2057.
- Hwang, J.S., Hsu, T.Y., 2000. Experimental study of isolated building under triaxial ground excitations. J. Struct. Eng. 126 (8), 879–886.
- Islam, M., Ellingwood, B., Corotis, R.B., 1992. Wind-induced response of structurally asymmetric high-rise buildings. J. Struct. Eng. 118 (1), 207–222.
- Jangid, R.S., Kelly, J.M., 2000. Torsional displacements in base-isolated buildings. Earthq. Spectra 16 (2), 443–454.

- JSSI (Japan Society of Seismic Isolation), 2017. Guidelines for Wind-Resistance Design of Base-Isolated Buildings. JSSI, Tokyo.
- Kareem, A., 1985. Lateral-torsional motion of tall buildings to wind loads. J. Struct. Eng. 111 (11), 2479–2496.
- Kareem, A., 1997. Modelling of base-isolated buildings with passive dampers under winds. J. Wind Eng. Ind. Aerod. 72, 323–333.
- Katagiri, J., Ohkuma, T., Yasui, H., Marukawa, H., Tsurumi, T., 2011. Study of accuracy for reduced model of high-rise buildings with base isolation systems. AIJ J. Technol. Des. 17 (36), 461–466 (In Japanese).
- Katagiri, J., Ohkuma, T., Marukawa, H., Yasui, H., 2012. Unstable aerodynamic responses of base-isolated high-rise buildings. J. Struct. Construct. Engi. AIJ 77 (681), 1637–1644 (In Japanese).
- Katagiri, J., Ohkuma, T., Marukawa, H., Tsurumi, T., 2014. Study of wind response of isolated layer of a base-isolated high-rise building using rain-flow method. Tokyo, Japan. In: Proceedings of 23rd National Symposium on Wind Engineering, pp. 307–312 (In Japanese).
- Kijewski, T., Kareem, A., 1998. Dynamic wind effects: a comparative study of provisions in codes and standards with wind tunnel data. Wind Struct. 1 (1), 77–109.
- Lee, C.S., Hong, H.P., 2010. Statistics of inelastic responses of hysteretic systems under bidirectional seismic excitations. Eng. Struct. 32 (8), 2074–2086.
- Liang, B., Shishu, X., Jiaxiang, T., 2002. Wind effects on habitability of base-isolated buildings. J. Wind Eng. Ind. Aerod. 90 (12–15), 1951–1958.
- Nagarajaiah, S., Reinhorn, A.M., Constantinou, M.C., 1991. Nonlinear dynamic analysis of 3-D-base-isolated structures. J. Struct. Eng. 117 (7), 2035–2054.
- Nagarajaiah, S., Reinhorn, A.M., Constantinou, M.C., 1993. Torsion in base-isolated structures with elastomeric isolation systems. J. Struct. Eng. 119 (10), 2932–2951.
- Ogawa, R., Yoshie, K., Sato, D., Sato, T., Kitamura, H., 2016. Prediction method for quasi-static component response of high-rise seismic isolated building under fluctuating wind force. J. Wind Eng. 41 (2), 41–47 (In Japanese).
- Pan, T.C., Kelly, J.M., 1983. Seismic response of torsionally coupled base isolated structures. Earthq. Eng. Struct. Dynam. 11 (6), 749–770.
- Park, Y.J., Wen, Y.K., Ang, A.H.S., 1986. Random vibration of hysteretic systems under bi-directional ground motions. Earthq. Eng. Struct. Dynam. 14 (4), 543–557.
- Roberts, J.B., Spanos, P.D., 2003. Random Vibration and Statistical Linearization. Dover Publications, Mineola, NY.
- Ryan, K.L., Polanco, J., 2008. Problems with Rayleigh damping in base-isolated buildings. J. Struct. Eng. 134 (11), 1780–1784.
- Shimada, K., Tamura, Y., Fujii, K., Wakahara, T., 1990. Wind induced torsional motion of tall building. In: Proceedings of 11th National Symposium on Wind Engineering, pp. 221–226 (in Japanese).
- Seguín, C.E., Juan, C., Almazán, J.L., 2008. Base–structure interaction of linearly isolated structures with lateral–torsional coupling. Eng. Struct. 30 (1), 110–125.

- Seguin, C.E., Almazán, J.L., Juan, C., 2013. Torsional balance of seismically isolated asymmetric structures. Eng. Struct. 46, 703–717.
- Shinozuka, M., Jan, C.M., 1972. Digital simulation of random processes and its applications. J. Sound Vib. 25 (1), 111–128.
- Shyamsunder, L., Pandey, D.K., Mishra, S.K., 2021. Behavior of torsionally coupled buildings isolated by super-elastic bearing subjected to earthquakes. J. Build. Eng. 43, 102573.
- Siringoringo, D.M., Fujino, Y., 2017. Wind-induced responses and dynamics characteristics of an asymmetrical base-isolated building observed during typhoons. J. Wind Eng. Ind. Aerod. 167, 183–197.
- Tallin, A., Ellingwood, B., 1985. Wind induced lateral-torsional motion of buildings. J. Struct. Eng. 111 (10), 2197–2213.
- Tokyo Polytechnic University (TPU), 2021. Wind pressure Database for high-rise building. URL. http://www.wind.arch.t-kougei.ac.jp/system/eng/contents/code/tp
- Wang, C.H., Wen, Y.K., 2000. Evaluation of pre-Northridge low-rise steel buildings. I: Modeling. J. Struct. Eng. 126 (10), 1160–1168.
- Wen, Y.K., 1976. Method for random vibration of hysteretic systems. J. Eng. Mech. Div. 102 (2), 249–263.